To the Graduate Council,

I am submitting herewith a thesis written by Harold H. Yount entitled "The Exact Solution of the Rayleigh Scattering Theory for Circular Cylinders as a Design Aid to the Development of Particle Sizing Instruments." I recommend that it be accepted in partial fulfillment of the requirements for the degree of Master of Science, with a major in Electrical Engineering.

T.V. Blalock

T.V. Blalock, Major Professor

We have read this thesis
and recommend its acceptance:

Robert E. Bolinkemeier

James Rochelle

Accepted for the Council:

Vice Provost
and Dean of The Graduate School

STATEMENT OF PERMISSION TO USE

In presenting this thesis in partial fulfillment of the requirements for a Master's degree at The University of Tennessee, Knoxville, I agree that the Library shall make it available to borrowers under rules of the Library. Brief quotations from this thesis are allowable without special permission, provided that accurate acknowledgment of the source is made.

Permission for extensive quotation from or reproduction of this thesis may be granted by my major professor, or in his absence, by the Head of Interlibrary Services when, in the opinion of either, the proposed use of the material is for scholarly purposes. Any copying or use of the material in this thesis for financial gain shall not be allowed without my written permission.

Signature Harold H Yount

Date 9 November 1989

THE EXACT SOLUTION OF THE RAYLEIGH SCATTERING THEORY FOR CIRCULAR CYLINDERS AS A DESIGN AID TO THE DEVELOPMENT OF PARTICLE SIZING INSTRUMENTS

A Thesis
Presented for the
Master of Science
Degree
The University of Tennessee, Knoxville

Harold H. Yount
December 1989

ACKNOWLEDGMENTS

The author wishes to acknowledge Dr. T. V. Blalock for his valuable assistance and encouragement throughout the course of this research and preparation of this thesis. Drs. R. Bodenheimer and J. Rochelle have also been very helpful in their capacities as members of the committee.

Special appreciation is extended to Dr. F. M. Shofner and Schaffner Technologies, Inc. for the unique opportunities, assistance, and funding which made this research possible.

The author sincerely appreciates the patience and encouragement of his immediate family and all of their assistance through this course of study.

ABSTRACT

An exact solution of Maxwell's equations for the diffraction created by a non-conducting cylinder in a propagating plane wave at normal incidence is presented. The exact solution contains a series of Bessel functions with argument ka (where k is the wave number and a is the radius of the cylinder). In previous work, this solution was not suited for numerical calculation for large values of ka because of the slow convergence of the series. An algorithm has been developed which will allow computation of this exact solution even for large values of ka. This theoretical work is presented as an aid in the design of instruments intended to measure properties of airborne particles based on their optical response.

The algorithm has been applied to the case of glass fibers whose diameters range from approximately one-half to twenty micrometers. The design goal was to develop an optical sensor using near infrared radiation that would have a linear response as a function of diameter over the range of interest. Theoretical calculations showed that the total power scattered by the fiber into a specific region would have the desired relationship with diameter. An optical sensor was built based upon the design indicated and tested to verify the response. A very high correlation was found to exist between the diameter as predicted by the sensor and the diameter measured microscopically.

TABLE OF CONTENTS

CHAPTER		PAGE
I.	INTRODUCTION	1
	Problem Definition	1
	Principals of Rayleigh Scattering	2
	Principals of the Simulation of Rayleigh's Theory	2
	Results of the Simulation of Rayleigh's Theory	4
	Results of the Experiment	4
II.	THE EXACT SOLUTION OF THE SCATTERING OF A PLANE ELECTROMAGNETIC WAVE BY A CIRCULAR CYLINDER	6
	Basis of the Derivation	6
	General Theory	8
	Perpendicular Incidence and Non-Polarized Radiation	14
III.	DEVELOPMENT OF AN ALGORITHM FOR THE CALCULATION OF THE EXACT SOLUTION FOR LARGE RADIUS CYLINDERS	16
	Fundamental Difficulties with the Solution	16
	Limiting the Infinite Summation	16
	Computation of Bessel Functions of Integer Order	17
	Calculation of the Scattered Intensity at a Point	19
	Calculation of the Average Intensity in a Region of Space	20
IV.	RESULTS OF THE CALCULATION OF THE THEORETICAL SOLUTION FOR GLASS CYLINDERS	23
	Basic Assumptions and Physical Limitations	23
	Explanation of Scattering Diagrams	24
	Calculation of the Total Power Scattered into a Region	24
	Linearity of the Response Function	25

CHAPTER PAGE

V. DESIGN OF THE OPTICAL SENSOR BASED ON THEORETICAL RESULTS 28
Design Constraints 28
Generation of the Planar Wavefront 28
Measurement of the Total Power Scattered into the Region of Interest 33
Analog Signal Processing 35
VI. EXPERIMENTAL RESULTS 37
Test Circuitry 37
Fiber Preparation 37
Correlation of the Results with Theory 39
VII. CONCLUSION 42
General Summary 42
Areas for Further Study 42
LIST OF REFERENCES 43
APPENDICES 45
Appendix A 46
Appendix B 58
VITA 79

LIST OF FIGURES

FIGURES	PAGE
1. General Configuration of the Cylinder and Coordinate System with Modes of Incident Radiation	7
2. Cylindrical Scatterer with Propagating Wave	21
3. Theoretical Average Intensity Over the 30^0-50^0 Range versus Cylinder Diameter	26
4. Optical Arrangement for the Generation of the Propagating Wave	30
5. Radiation Pattern of the Motorola Diode	31
6. Ray Approximation to the Propagating Plane Wave in a) the X-Y Plane and b) the X-Z Plane	32
7. Optical Arrangement for the Collection of the Scattered Power	34
8. Basic Circuit for the Analog Signal Processing	36
9. Directly Coupled Circuit for Static Testing	38
10. Experimental Average Intensity Over the 30^0-50^0 Range versus Cylinder Diameter	40
11. Theoretical Plot of Intensity versus Angle for Cylinders of 1 um Diameter	59
12. Theoretical Plot of Intensity versus Angle for Cylinders of 2 um Diameter	60
13. Theoretical Plot of Intensity versus Angle for Cylinders of 3 um Diameter	61
14. Theoretical Plot of Intensity versus Angle for Cylinders of 4 um Diameter	62
15. Theoretical Plot of Intensity versus Angle for Cylinders of 5 um Diameter	63
16. Theoretical Plot of Intensity versus Angle for Cylinders of 6 um Diameter	64
17. Theoretical Plot of Intensity versus Angle for Cylinders of 7 um Diameter	65

FIGURES PAGE

18. Theoretical Plot of Intensity versus Angle for Cylinders of 8 um Diameter 66
19. Theoretical Plot of Intensity versus Angle for Cylinders of 9 um Diameter 67
20. Theoretical Plot of Intensity versus Angle for Cylinders of 10 um Diameter 68
21. Theoretical Plot of Intensity versus Angle for Cylinders of 11 um Diameter 69
22. Theoretical Plot of Intensity versus Angle for Cylinders of 12 um Diameter 70
23. Theoretical Plot of Intensity versus Angle for Cylinders of 13 um Diameter 71
24. Theoretical Plot of Intensity versus Angle for Cylinders of 14 um Diameter 72
25. Theoretical Plot of Intensity versus Angle for Cylinders of 15 um Diameter 73
26. Theoretical Plot of Intensity versus Angle for Cylinders of 16 um Diameter 74
27. Theoretical Plot of Intensity versus Angle for Cylinders of 17 um Diameter 75
28. Theoretical Plot of Intensity versus Angle for Cylinders of 18 um Diameter 76
29. Theoretical Plot of Intensity versus Angle for Cylinders of 19 um Diameter 77
30. Theoretical Plot of Intensity versus Angle for Cylinders of 20 um Diameter 78

CHAPTER I

INTRODUCTION

1.1 PROBLEM DEFINITION

The basic problem involved in this research is the accurate and repeatable measurement of the length and diameter of small glass fibers. These fibers typically range in diameter from one-half to twenty micrometers and in length from five-hundred to four-thousand micrometers. They are presented for measurement supported in an air stream with an average velocity of approximately 50 meters per second. The fibers are known to be oriented such that the axis of the cylinder is parallel to the direction of air flow and are separated by approximately five centimeters in the air stream.

The fibers themselves are the product of a fiberglass spinning process. Basic assumptions include a glass index of refraction of 1.5 with a negligible absorption component and nearly perfect cylindrical fibers. This information is supplied by the manufacturer and is borne out by the experiment.

The approach taken to make this measurement involves the use of light scattering. The fibers supported in the air stream are transported through a plane wave of incoherent light. The total light scattered by the fiber into a collection system is measured and correlated to the fiber diameter. Since the fibers are in motion through the light beam, the signal resulting from the collection system resembles closely an ideal pulse. The duration of the pulse is a function of the time of flight of the fiber through the plane wave which relates directly to the length of the fiber. The amplitude of the pulse is a function of the diameter of the fiber.

1.2 PRINCIPALS OF RAYLEIGH SCATTERING

The Rayleigh scattering theory is a particular solution of Maxwell's equations for electromagnetic fields; in this situation, the solution is for the special case of an infinite cylinder obstructing a narrow incident wave. Rayleigh establishes the intensity of scattered light at some point in space as a function of a) the intensity and wavelength of the incident wave, b) the diameter and refractive index of the cylinder, c) the distance between the cylinder axis and the point, and d) the angle that a ray from the cylinder to the point makes with the direction of incident wave propagation.[1] Since the fiber is in fact a cylinder, the scattered light is confined to the plane perpendicular to the axis of the cylinder. The validity of the theory has been shown in several published experiments.[2] The basic equation developed from Rayleigh's theorem is valid only for light which has been polarized parallel to the plane of the scattering. A similar equation for polarization parallel to the cylinder's axis may also be developed. For the case of an unpolarized incident wave, however, the solution contains fractional portions of the two polarized solutions since natural light is comprised of equal components of polarization.[3] Rayleigh's original development corresponds to scattering from a spherical object. Modification to allow for a cylindrical scatterer is very straightforward and only modifies the dependence on the distance from the scatterer. Intuitively, a spherical object radiates in all three dimensions; therefore the intensity must decrease as the square of the distance. A cylinder radiates only in two dimensions, so the intensity falls off linearly with the distance.

1.3 PRINCIPALS OF THE SIMULATION OF RAYLEIGH'S THEORY

The primary goal of the simulation program is the calculation of the scattering coefficients and subsequently the intensity of light scattered to a particular point. These calculations are used to

predict the linearity of the power collected in a particular solid angle as a function of fiber diameter. Since the scattering from a fiber with the axis oriented along the z-axis of a cartesian coordinate system is contained entirely in the x-y plane, the solid angles under consideration may be simplified to two-dimensional angles.

Once the basic parameters such as the wavelength (λ), diameter (d), and index of refraction (m) have been assigned, the real work lies in the calculation of various Bessel functions. Rayleigh's equation is essentially a ratio of Bessel function sums with two different arguments; the arguments are *ka* and *mka*. In this case, the index of refraction of the fiber is known to be 1.5 with no absorption; the tedious calculation of Bessel functions with complex arguments is thereby avoided. The method of Bessel function generation employed is that suggested in reference [4] and amounts to the following steps. First, the approximation that the result of the Bessel of a much higher order is equal to zero is made; also the next lower order is assigned a one. Results can be computed for successively lower orders using the recursion relationship until the zeroth order is reached. Final results may then be obtained by normalizing the series. This rather elaborate method is employed in order to avoid the accumulation of the significant rounding errors that would otherwise have occurred with the use of forward recursion. As a matter of verification, the basic recursion relationship may be used to check that all results up to the order of interest are correct. Once the basic J and N functions have been computed for both arguments, other functions such as the Hankel of the second kind and the derivatives of the above functions may be readily generated.

The calculation of intensity versus angle for a particular set of physical parameters proceeds rapidly after the generation of the appropriate Bessel functions. Total power scattered into a range of angles is simply the integral of the intensity function over those angles. Another approach is to calculate the average intensity in the

region and multiply by the area of the region. Intensities are calculated for every tenth of a degree to yield a meaningful average.

1.4 RESULTS OF THE SIMULATION OF RAYLEIGH'S THEORY

After plotting power versus diameter for many ranges of angles, the most useful arrangement was found to be the collection of all light scattered in the plane perpendicular to the fiber axis from thirty to fifty degrees away from the direction of propagation. A nearly linear relationship as calculated using a least squares best fit line with a correlation coefficient of R = 0.9979 between power and diameter is found for this range. From this data, a sensing unit collecting 30-50 degrees has been designed and implemented for testing the power versus diameter relationship. Other sets of angles approaching ninety degrees were also found, but the 30-50 degree range was selected as being the most practical for implementation.

1.5 RESULTS OF THE EXPERIMENT

After developing an optical sensor based on the results of the simulation, an experiment was run to verify that the sensor performance was satisfactory. The sensor itself is composed of three main sections, namely the source optics, the detection optics, and the sampling volume. The function of the source optics is to generate a wavefront propagating in the direction of the sampling volume. For the purposes of the experiment, individual glass fibers of known diameters were inserted into the beam present in the sampling volume. All light scattered by the fiber between 30-50 degrees (measured from the direction of beam propagation) is collected by the detection optics and focused onto a large area PIN diode structured optical detector. The current generated by such a detector is directly proportional to the incident optical power. To facilitate the measurement of this current, a transimpedance

amplifier with a total DC gain of 30×10^6 V/A with a low-pass characteristic frequency response was used in conjunction with a digital volt meter.

Fibers whose diameters range from 1 um to 23 um were measured with the above experimental set-up. Voltages measured for these fibers range from 0.49V to 5.73V. Again, a linear relationship between voltage (proportional to incident optical power) and diameter was found using a least squares best fit line with a correlation coefficient of R = 0.9977.

CHAPTER II

THE EXACT SOLUTION OF THE SCATTERING OF A PLANE ELECTROMAGNETIC WAVE BY A CIRCULAR CYLINDER

2.1 BASIS OF THE DERIVATION

In order to use the boundary value method to obtain the solution, the surface of the scatterer should correspond to a complete coordinate surface and the coordinate system chosen should be one in which the wave equation is separable. Since this solution is to be derived for the case of cylindrical scatterers, it is appropriate that the cylindrical coordinate system be utilized. The cylindrical coordinates, r, θ, z, are illustrated in Fig. 1 along with their relationship to the cartesian system. The figure also shows a representation of the cylindrical scatterer and the electromagnetic vectors for the transverse electric (TE) and transverse magnetic (TM) fields at oblique incidence. Note that the cylinder axis is taken to be coincident with the z-axis. A simplified case occurs when the incident plane wave of unit intensity propagates perpendicularly to the z-axis.

In the more general case of oblique incidence, the incident plane wave direction of propagation makes an angle Φ with respect to the normal of the z-axis. The polarized incident wave may be resolved into two components: a) the TM mode for which there is no z-component of the magnetic vector and b) the TE mode for which there is no z-component of the electric vector. In other words, the TM mode has its magnetic vector vibrating perpendicularly to the plane formed by the incident wave and the z-axis, while the TE mode's electric vector vibrates perpendicular to this plane.

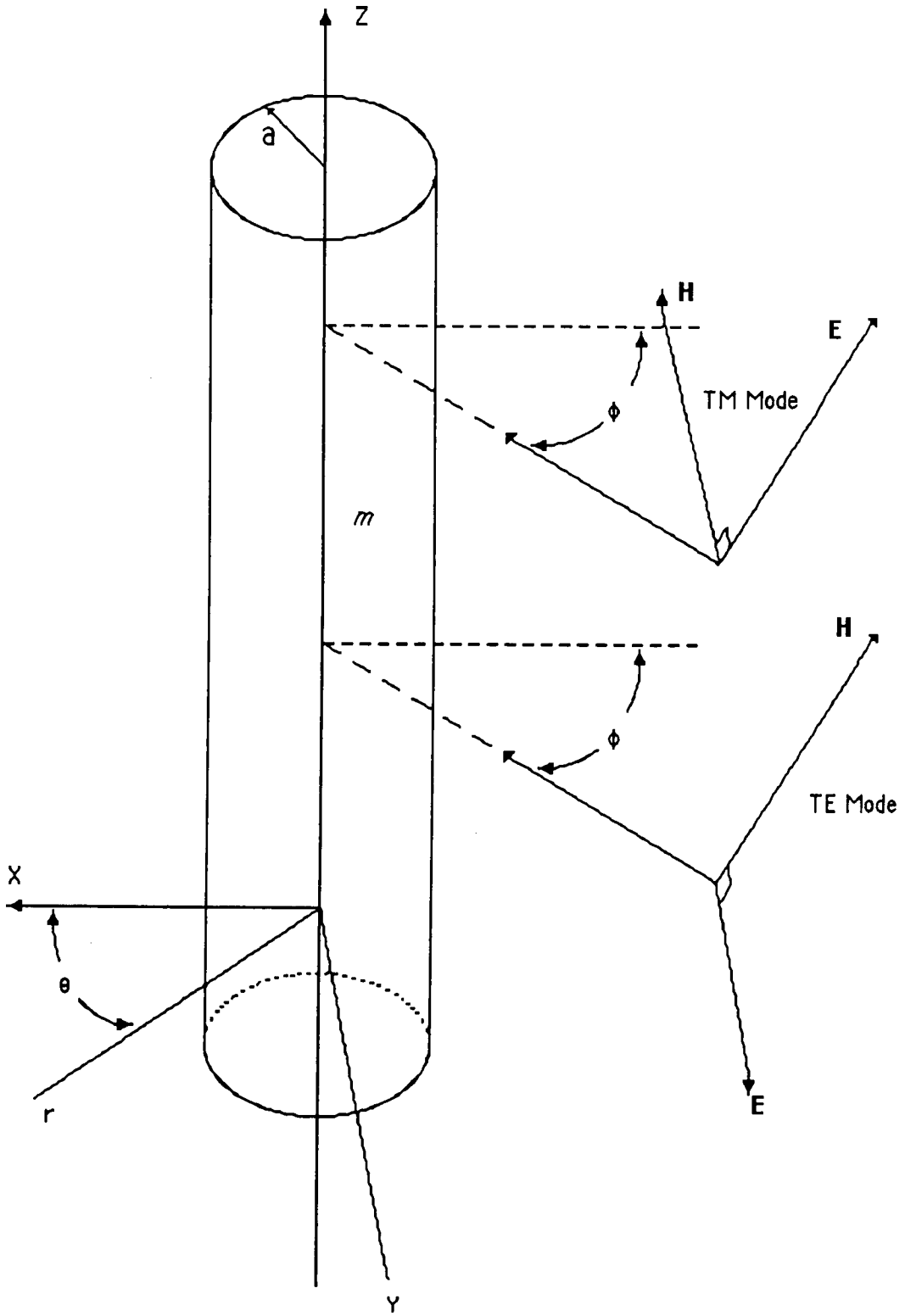


Figure 1. General Configuration of the Cylinder and Coordinates with Modes of Incident Radiation

2.2 GENERAL THEORY

The theoretical derivation of the light scattering equations that follows was originally derived by Lord Rayleigh in the late 19th century. The field vectors corresponding to each of the modes of propagation illustrated in Figure 1 can be related to a scalar potential which in turn satisfies the scalar wave equation. In cylindrical coordinates, this is

$$\frac{1}{r}\frac{\delta}{\delta r}\left[\frac{r\delta\Pi}{\delta r}\right] + \frac{1}{r^2}\frac{\delta^2\Pi}{\delta z^2} + k^2\Pi = 0. \qquad (2.1)$$

The function Π can be written as a product of three factors, each of which is a function of only one coordinate variable and satisfies the following ordinary differential equations :

$$r\frac{\delta}{\delta r}\left[\frac{r\delta R(r)}{\delta r}\right] + \left[(k_o^2 - k^2)\, r^2 - n^2\right] R(r) = 0, \qquad (2.2)$$

$$\frac{\delta^2\Theta(\theta)}{\delta\theta^2} + n^2\,\Theta(\theta) = 0 \quad \text{and,} \qquad (2.3)$$

$$\frac{\delta^2 Z(z)}{\delta z^2} + h^2 Z(z) = 0, \qquad (2.4)$$

$$\text{where} \quad h = k_0 \sin\phi. \qquad (2.5)$$

The potential functions within the homogeneous cylinder of refractive index *m* must now be constructed from an appropriate superposition of

$$\Pi_n = e^{(i\omega t + in\theta - ihz)}\left[Z_n r\sqrt{m^2k_o^2 - h^2}\right], \qquad (2.6)$$

where each term represents a solution for each of the above ordinary differential equations. As in Van de Hulst [5], m is defined as the refractive index of the cylinder and k_o is the propagation constant outside the cylinder. The medium surrounding the cylinder is treated as if it were a vacuum. If the surrounding medium were not a vacuum, m would necessarily become the refractive index of the cylinder relative to that of the medium.

The radial equation (2.2) has two independent solutions: J_n, the integral order Bessel function of the first kind, and N_n, the integral order Neumann function (Bessel function of the second kind) where the index n takes on integral values. The corresponding Hankel functions are constructed as shown[6]:

$$H_n^{(2)} = J_n - iN_n , \tag{2.7}$$

$$J_n(z) = \sum_{m=0}^{\infty} \frac{(-1)^m}{m!\ \Gamma\ (m + n + 1)} \left[\frac{z}{2}\right]^{n+2m} \quad \text{and,} \tag{2.8}$$

$$N_n = \frac{2}{\pi}\left\{J_n(z)\ (\gamma + \ln\ (z/2)\ )\right\} - \frac{1}{\pi}\sum_{m=0}^{n-1} \frac{(n-m-1)!}{m!} \left[\frac{z}{2}\right]^{2m-n}$$

$$+ \frac{1}{\pi}\sum_{m=0}^{n-1} \frac{(-1)^{m+1}}{m!(m+n)!}\ (z/2)^{2m+n}\ \left\{\phi(k) + \phi(n+k)\right\} . \tag{2.9}$$

The potential for the total wave outside the cylinder ($r > a$) is obtained by summing two functions, one of which represents the incident wave while the other represents the scattered wave. The incident wave traveling in the direction shown in Fig. 1 is represented by

$$\Pi_i = e^{[i\omega t - ik_0 (x \cos\phi + z \sin\phi)]}$$

$$= e^{[i\omega t - ihz]} \sum_{n=0}^{\infty} (-i)^n J_n(\ell r) e^{in\theta}, \qquad (2.10)$$

where

$$\ell = \sqrt{k_o^2 - h^2} = k_o \cos\phi. \qquad (2.11)$$

This wave may be resolved into two separate components corresponding to the TM mode and the TE mode of propagation. When the incident wave is perpendicular to the cylinder axis ($\Phi = 0$), incident TE waves scatter in a transverse-electric mode and incident TM waves scatter in a TM mode. However, for oblique incidence ($\Phi \neq 0$) the incident TE waves are partially rotated into TM scattered waves and similarly, the incident TM waves are partially rotated into TE scattered waves. In order to apply the boundary conditions, it is necessary to generate both TM and TE mode solutions in the internal and scattered waves corresponding to each case in the incident wave. Accordingly, the potential functions may be set up using the Hertz vectors as follows :

TM Mode

$r > a$:

$$u_{TM} = \sum_{n=0}^{\infty} F_n \{ J_n(\ell r) - b_{nTM} H_n^{(2)}(\ell r) \} \qquad (2.12)$$

$$v_{TM} = \sum_{n=0}^{\infty} F_n \{ a_{nTM} H_n^{(2)}(\ell r) \} \qquad (2.13)$$

$r < a$:

$$u_{TM} = \sum_{n=0}^{\infty} F_n \{ d_{nTM} J_n(jr) \} \qquad (2.14)$$

$$v_{TM} = \sum_{n=0}^{\infty} F_n \{ c_{nTM} J_n(jr) \} \quad (2.15)$$

TE Mode

$r > a$:

$$u_{TE} = \sum_{n=0}^{\infty} F_n \{ b_{nTE} H_n^{(2)}(\ell r) \} \quad (2.16)$$

$$v_{TE} = \sum_{n=0}^{\infty} F_n \{ J_n(\ell r) - a_{nTE} H_n^{(2)}(\ell r) \} \quad (2.17)$$

$r < a$:

$$u_{TE} = \sum_{n=0}^{\infty} F_n \{ d_{nTE} J_n(jr) \} \quad (2.18)$$

$$v_{TE} = \sum_{n=0}^{\infty} F_n \{ c_{nTE} J_n(jr) \} \quad (2.19)$$

where

$$F_n = (-i)^n e^{i(\omega t - hz + n\theta)} \quad (2.20)$$

and,

$$j = \sqrt{m^2 k_o^2 - h^2} \quad . \quad (2.21)$$

In order to yield physically realizable solutions, the boundary conditions must be that the tangential components of the electric field *E* and the magnetic field *H* be continuous at the cylinder surface ($r = a$); this requires the continuity of the following expressions at the surface :

$$\frac{\delta v}{\delta r} + \frac{inh}{mk_o r} u \,, \tag{2.22}$$

$$\frac{m^2 k_o^2 - h^2}{mk_o} u \,, \tag{2.23}$$

$$m \frac{\delta u}{\delta r} - \frac{inh}{k_o r} v \quad \text{and,} \tag{2.24}$$

$$(m^2 k_o^2 - h^2) v \,. \tag{2.25}$$

Solving these boundary conditions leads to eight sets of linear algebraic equations which can be solved for the scattering coefficients as follows :

$$a_{nTM} = \Delta^{-1} \begin{vmatrix} \frac{-ihn}{\alpha} J_n(\ell a) & \frac{-ihn}{m\alpha} J_n(ja) & \frac{-ihn}{\alpha} H_n^{(2)}(\ell a) & -jJ_n'(ja) \\ \frac{-\ell^2}{k_o} J_n(\ell a) & \frac{-j^2}{mk_o} J_n(ja) & \frac{-\ell^2}{k_o} H_n^{(2)}(\ell a) & 0 \\ -\ell J_n'(la) & -mjJ_n'(ja) & -\ell H_n^{(2)'}(\ell a) & \frac{ihn}{\alpha} J_n(ja) \\ 0 & 0 & 0 & -j^2 J_n(ja) \end{vmatrix} \tag{2.26}$$

$$b_{nTM} = \Delta^{-1} \begin{vmatrix} \ell H_n^{(2)'}(\ell a) & \frac{ihn}{m\alpha} J_n(ja) & \frac{ihn}{\alpha} J_n(\ell a) & -jJ_n'(ja) \\ 0 & \frac{-j^2}{mk_o} J_n(ja) & \frac{-\ell^2}{k_o} J_n(\ell a) & 0 \\ \frac{-ihn}{\alpha} H_n^{(2)}(\ell a) & -mjJ_n'(ja) & -\ell J_n'(\ell a) & \frac{ihn}{\alpha} J_n(ja) \\ \ell^2 H_n^{(2)}(\ell a) & 0 & 0 & -j^2 J_n(ja) \end{vmatrix} \tag{2.27}$$

$$a_{nTE} = \Delta^{-1} \begin{vmatrix} -\ell J_n'(\ell a) & \frac{-ihn}{m\alpha} J_n(ja) & \frac{ihn}{\alpha} H_n^{(2)}(\ell a) & -jJ_n'(ja) \\ 0 & \frac{-j^2}{mk_o} J_n(ja) & \frac{\ell^2}{k_o} H_n^{(2)}(\ell a) & 0 \\ \frac{ihn}{\alpha} J_n(\ell a) & -mjJ_n'(ja) & \ell H_n^{(2)'}(\ell a) & \frac{ihn}{\alpha} J_n(ja) \\ -\ell^2 J_n(\ell a) & 0 & 0 & -j^2 J_n(ja) \end{vmatrix} \qquad (2.28)$$

$$b_{nTE} = \Delta^{-1} \begin{vmatrix} -\ell H_n^{(2)'}(\ell a) & \frac{-ihn}{m\alpha} J_n(ja) & -\ell J_n'(\ell a) & -jJ_n'(ja) \\ 0 & \frac{-j^2}{mk_o} J_n(ja) & 0 & 0 \\ \frac{ihn}{\alpha} H_n^{(2)}(\ell a) & -mjJ_n'(ja) & \frac{ihn}{\alpha} J_n(\ell a) & \frac{ihn}{\alpha} J_n(ja) \\ -\ell^2 H_n^{(2)}(\ell a) & 0 & -\ell^2 J_n(\ell a) & -j^2 J_n(ja) \end{vmatrix} \qquad (2.29)$$

where

$$\Delta = \begin{vmatrix} \ell H_n^{(2)'}(\ell a) & \frac{-ihn}{m\alpha} J_n(ja) & \frac{-ihn}{\alpha} H_n^{(2)}(\ell a) & -jJ_n'(ja) \\ 0 & \frac{-j^2}{mk_o} J_n(ja) & \frac{-\ell^2}{k_o} H_n^{(2)}(\ell a) & 0 \\ \frac{ihn}{\alpha} H_n^{(2)}(\ell a) & -mjJ_n'(ja) & -\ell H_n^{(2)'}(\ell a) & \frac{ihn}{\alpha} J_n(ja) \\ \ell^2 H_n^{(2)}(\ell a) & 0 & 0 & -j^2 J_n(ja) \end{vmatrix} \qquad (2.30)$$

The intensity functions in the far-field are then given by

$$I_{TM-TM} = \frac{2}{k_0 \pi r} |T_{TM-TM}|^2 = \frac{2}{k_0 \pi r} \left| b_{0TM} + 2 \sum_{n=1}^{\infty} b_{nTM} \cos(n\theta) \right|^2 , \quad (2.31)$$

$$I_{TM-TE} = \frac{2}{k_0 \pi r} |T_{TM-TE}|^2 = \frac{2}{k_0 \pi r} \left| 2 \sum_{n=1}^{\infty} a_{nTM} \cos(n\theta) \right|^2 , \quad (2.32)$$

$$I_{TE-TM} = \frac{2}{k_0 \pi r} |T_{TE-TM}|^2 = \frac{2}{k_0 \pi r} \left| 2 \sum_{n=1}^{\infty} b_{nTE} \cos(n\theta) \right|^2 \text{ and,} \quad (2.33)$$

$$I_{TE-TE} = \frac{2}{k_0 \pi r} |T_{TE-TE}|^2 = \frac{2}{k_0 \pi r} \left| a_{0TE} + 2 \sum_{n=1}^{\infty} a_{nTE} \cos(n\theta) \right|^2 . \quad (2.34)$$

The following definitions apply : a) I_{TM-TM} is the TM mode intensity of the scattered radiation due to a TM mode incident wave, b) I_{TM-TE} represents the TE mode intensity of the scattered radiation due to a TM mode incident wave, c) I_{TE-TM} defines the TM mode intensity of the scattered wave from TE mode incident radiation, and d) I_{TE-TE} is the intensity of the TE mode scattered radiation from TE mode incident radiation.

2.3 PERPENDICULAR INCIDENCE AND NON-POLARIZED RADIATION

As mentioned previously perpendicular incidence requires that the angle Φ be equal to zero. Therefore,

$$h = 0, \quad \ell = k_0 \quad \text{and,} \quad k = mk_0 . \quad (2.35)$$

For this case, the cross-mode scattering terms reduce to zero such that

$$I_{TM\text{-}TE} = I_{TE\text{-}TM} = 0 , \tag{2.36}$$

and the scattering is given only by (2.31) and (2.34). The so-called scattering coefficients, a_n and b_n are given as

$$b_n = \frac{mJ_n(\alpha)J'_n(m\alpha) - J_n(m\alpha)J'_n(\alpha)}{mH_n^{(2)}(\alpha)J'_n(m\alpha) - J_n(m\alpha)H_n^{(2)'}(\alpha)} \quad \text{and} \tag{2.37}$$

$$a_n = \frac{J_n(\alpha)J'_n(m\alpha) - mJ_n(m\alpha)J'_n(\alpha)}{H_n^{(2)}(\alpha)J'_n(m\alpha) - mJ_n(m\alpha)H_n^{(2)'}(\alpha)} . \tag{2.38}$$

If the incident wave is non-polarized radiation as from an unfiltered light emitting diode, for instance, the wave is composed of two equally intense components polarized in the TE mode and the TM mode. Therefore, the complete expression for the scattered radiation from a uniform cylinder with perpendicular incidence of non-polarized light is given as the fractional sum of (2.31) and (2.34)

$$I = \frac{1}{k_0\pi r}\left|b_0 + 2\sum_{n=1}^{\infty} b_n\cos(n\theta)\right|^2 + \frac{1}{k_0\pi r}\left|a_0 + 2\sum_{n=1}^{\infty} a_n\cos(n\theta)\right|^2 , \tag{2.39}$$

where b_n and a_n are again given by (2.37) and (2.38) respectively. Since the scattered wave will propagate as a cylindrical wave originating from the z-axis, the intensity will fall off as the inverse of the radial distance.

CHAPTER III

DEVELOPMENT OF AN ALGORITHM FOR THE CALCULATION OF THE EXACT SOLUTION FOR LARGE RADIUS CYLINDERS

3.1 FUNDAMENTAL DIFFICULTIES WITH THE SOLUTION

The equation to be solved is given at the end of the previous chapter as (2.39). Note that in general, this equation is the infinite sum of a series of Bessel functions of increasing order but constant argument. In order to arrive at a solution, it is necessary to limit the summation to some upper bound that requires the series to converge within an acceptable range of its final value. For any given argument, the Bessel function of that argument tends toward zero with increasing order. Unfortunately, the rate at which the function approaches zero varies inversely with the magnitude of the argument. For cylinders whose radius is more than a few times the wavelength of the incident radiation, the series converges too slowly for convenient calculation. However, with the advent of today's higher speed and more cost effective computers, direct solution methods are employed that utilize many thousands more calculations than the hand approximations.

3.2 LIMITING THE INFINITE SUMMATION

In his 1966 paper, Kerker shows mathematically that the infinite summation of Bessel functions converges if an upper limit of (2.8 mka + 11) is imposed. [7] This is verifiable by computing the sum for the same argument to the limit of (4.3 mka + 11). The justification for the convergence is that $J_n(x)$ approaches zero as the ratio of n/x increases. In fact, when n/x is greater than three, $J_n(x)$ becomes smaller than 10^{-4}. The variable X corresponds to mka and ka in equation (2.39). Using the upper limit of (2.8 mka +

11) as n, produces n/x ratios of at least 2.8 and $2.8m$. Therefore the value of $J_n(x)$ is less than 10^{-4} at the upper limit of the summation. It should be noted that this is the most pessimistic example since for the n/x ratios of $2.8m$, $J_n(x)$ is much less than 10^{-4} at the limit. For the case of a twenty-five micrometer diameter glass cylinder with an index of refraction of 1.5 scattering near-infra-red radiation (wave-length of 840 nanometers), the upper limit calculates to 392. Therefore, the sum must be carried out for approximately four-hundred steps and Bessel functions must be computed for all orders from 0 to 400.

3.3 COMPUTATION OF BESSEL FUNCTIONS OF INTEGER ORDER

There are many different techniques for calculating the values of Bessel functions. Abramowitz and Stegun [5] give several sets of asymptotic expansions for different conditions such as large order or large arguments. Neither of the expansions holds for both large order and large arguments, however. There are also polynomial approximations which give very good results (error less than 10^{-8}) for specific ranges of arguments and for only the zeroth and first order functions. Unfortunately, since $J_n(x)$ is a decreasing function of n when $n > x$, the usual forward recursion relationship given in (3.1) accumulates significant rounding errors if it is used to calculate high order functions from the results of the polynomial approximations :

$$J_{n+1}(x) = \frac{2n}{x} J_n(x) - J_{n-1}(x) . \qquad (3.1)$$

There are also available many published tables of Bessel functions of integer order for orders up to twenty and arguments often as high as one-hundred. When accuracy is not critical, interpolation using these tables may be successfully employed.

When calculating the required Bessel functions for the solution of light scattering problems, however, all of the above methods have one or more serious drawbacks. The method employed in this application is also presented by Abramowitz and Stegun. Since $J_n(x)$ essentially vanishes for n larger than the upper limit as given in section 3.2, arbitrary values of zero and one are assigned to $J_n(x)$ for n equal to $(2.8\,mka + 11)$ and for n equal to $(2.8\,mka + 10)$, respectively. The recursion relation given in (3.1) then may be used to generate trial values for $J_n(x)$ as n approaches zero. These values should be rounded to the nearest integer at each step. Since $J_n(x)$ is an increasing function as n decreases, there is no accumulation of rounding errors in the trial values. Finally, the trial values must be normalized to yield valid results. The basic property given in equation (3.2) is used to find the normalization factor :

$$1 = J_0(x) + 2J_2(x) + 2J_4(x) + 2J_6(x) + \ldots \qquad (3.2)$$

Taking the inverse of the sum of the right side terms in (3.2) as this normalization factor and multiplying the trial values by this component yields the required results.

The calculation of the required Bessel functions of the second kind (Neumann functions) can be implemented in a simpler way. The polynomial approximations given by Abramowitz and Stegun give excellent results for the zeroth order solution. The Wronskian relation given in (3.3) is used to obtain the solution for the first order :

$$J_1(x)\,N_0(x) - J_0(x)\,N_1(x) = \frac{2}{\pi x}. \qquad (3.3)$$

With the zeroth and first order solutions completed, the forward recursion relation in (3.4) may be used to arrive at higher order solutions :

$$N_{n+1}(x) = \frac{2n}{x} N_n(x) - N_{n-1}(x) . \qquad (3.4)$$

Since the Neumann functions, $N_n(x)$, are not decreasing functions of n, there is no significant accumulation of rounding errors as in the case with the Bessel functions. This recursion should be carried out for orders up to the upper limit as calculated in section 3.1.

Note that the solution of equation (2.39) also requires the first derivatives with respect to the arguments of all the Bessel and Neumann functions. Equation (3.5) is used for the zeroth order derivatives, while (3.6) and (3.7) provide derivatives for higher orders :

$$J_0'(x) = -J_1(x) \; N_0'(x) = -N_1(x) , \qquad (3.5)$$

$$J_n'(x) = -J_{n+1}(x) + \frac{n}{x} J_n(x) , \qquad (3.6)$$

$$N_n'(x) = -N_{n+1}(x) + \frac{n}{x} N_n(x) . \qquad (3.7)$$

By the nature of the above computational methods all the required orders of Bessel and Neumann functions and their respective derivatives are calculated.

3.4 CALCULATION OF THE SCATTERED INTENSITY AT A POINT

The set of points in the cylindrical coordinate system for which the scattered intensity is not equal to zero is known as the scattering plane. As discussed previously, all the incident light scatters into planes that are perpendicular to the cylinder axis and contains that region of the cylinder upon which the light is incident. Therefore, the scattered intensity at any point in space not contained in the scattering plane is exactly zero. Taking the

direction of incident light propagation to be from the negative x-axis in Figure 2, the coordinates of any point in space with non-zero scattered intensity are given as :

$$r = \sqrt{x^2 + y^2}\ , \tag{3.8}$$

$$\theta = \tan^{-1}\left(\frac{y}{x}\right). \tag{3.9}$$

In this way, the values of r and θ as given above are exactly those required in (2.39) to give the total scattered intensity at that point. To compute the summations, the magnitudes are calculated and multiplied by the physical constants appropriate to the situation.

3.5 CALCULATION OF THE AVERAGE INTENSITY IN A REGION OF SPACE

Any given region of space is composed of an infinite number of points. If the scattered intensity of each and every point was known, an exact average intensity in the region could be theoretically calculated. More practically, if enough points to ensure that the intensity variation from point to point is a relatively smooth function are averaged, the difference from the exact value can be kept negligibly small. For the purposes of this exercise, it was determined that increments in space of one-tenth of one degree would be more than sufficient to minimize the error. This value was verified by computing the average using one one-hundredth of a degree increments. Observation of several scattering diagrams given in Appendix B shows that the variation of intensity as a function of angle is most dramatic for the larger cylinders. However, even for the twenty micrometer cylinders, the period of the variation is no less than about five degrees. Therefore, one-tenth degree increments provide a minimum of fifty data points per period.

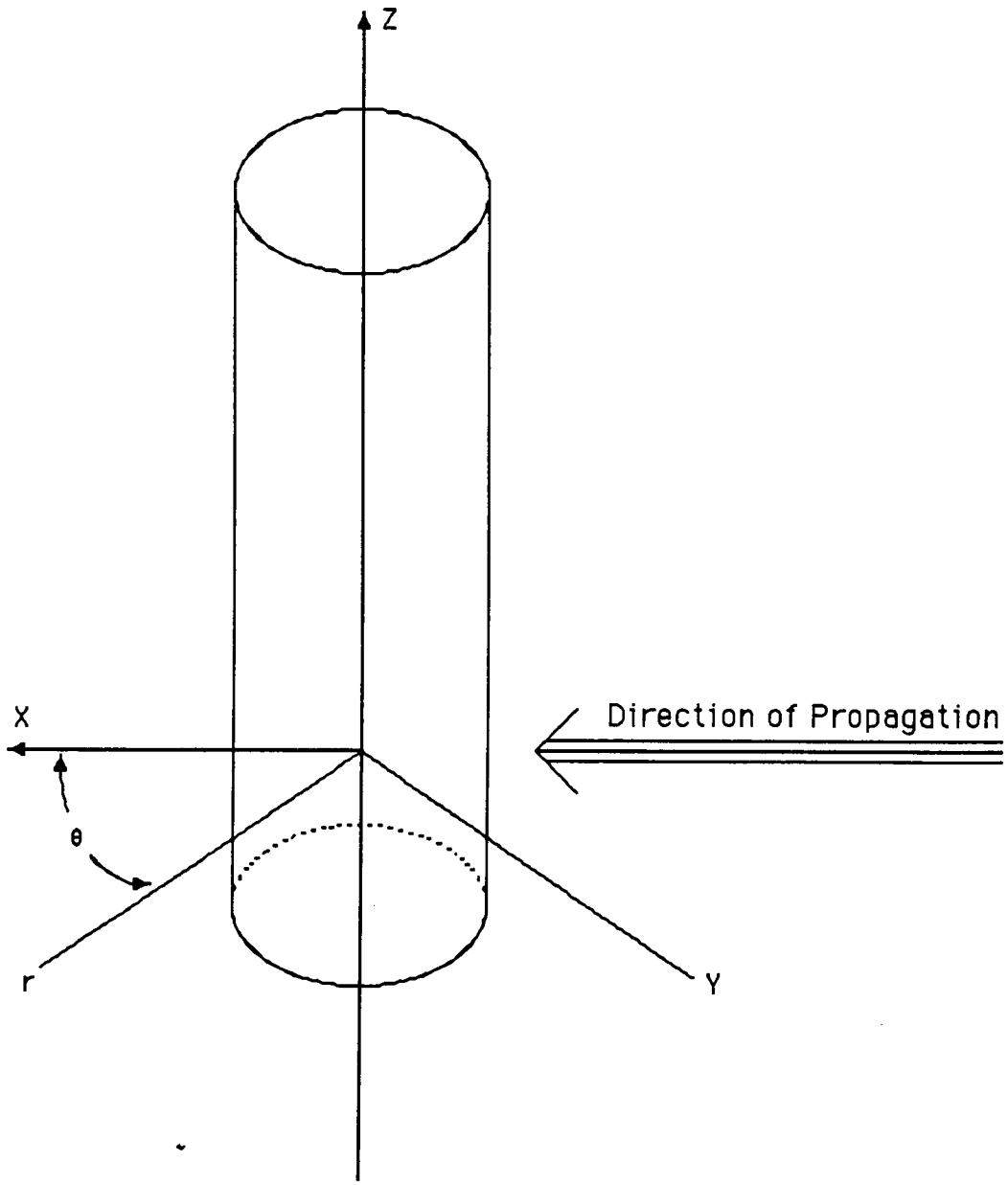


Figure 2. Cylindrical Scatterer with Propagating Wave

This solution is developed as an aid in designing practical optical instruments. These designs almost always incorporate a detector such as a PIN diode or photo-multiplier tube which inherently measures the power incident upon the device. By their nature, these devices measure only the average intensity (multiplied by the area obstructed) across a range of angles, rather than across a range of radii from the scatterer. Therefore, it is not necessary to calculate the average intensity across a range of radii.

As just implied, optical detectors invariably respond to the total incident power upon the detector, not the average intensity. However, for a given measurement scheme, the region of space being observed is fixed. Therefore, the total area also is fixed. Since the average intensity in this area multiplied by the area is the total power, the detector effectively responds to the average intensity.

CHAPTER IV

RESULTS OF THE CALCULATION OF THE THEORETICAL SOLUTION FOR GLASS CYLINDERS

4.1 BASIC ASSUMPTIONS AND PHYSICAL LIMITATIONS

Before the equations developed in Chapters 2 and 3 can be made useful, it is necessary to establish the basic parameters of the sensing unit being designed. The intent is to develop a sensor capable of measuring the diameter of glass fibers. These fibers may be considered as very nearly perfect cylinders with a constant refractive index. The diameter from fiber to fiber may vary over the entire range from one-half to twenty micrometers, but the diameter of a single fiber will not vary significantly over its length. Observation using a microscope with a magnification of 1000x of many hundreds of these glass fibers confirmed the constant diameter. The index of refraction of the glass is known to be very close to 1.5, with no absorption.

Since optical detectors, especially PIN diodes, are relatively small, it is necessary to use a lens system to collect all of the scattered light and focus it on the detector surface. There is a practical limit to the amount of light which may be collected by any given lens system, however. Since in this case it is desired to design such that the detector is on the axis of propagation of the incident beam, scattering at angles greater than about sixty degrees would require a rather complex system to be focused onto the detector. The wider the angle, of course, the larger the lens diameter must be and the closer the lens must be located to the scatterer. The fresnel lens offers a unique combination of large diameters with very short focal lengths.

4.2 EXPLANATION OF SCATTERING DIAGRAMS

Appendix B contains the results of the calculations of Chapters 2 and 3. The calculations were performed with the above assumptions about the fibers and for a continuous range of angles between 0 and 90 degrees from the x-axis. The most convenient form in which to present the data is known as a scattering diagram. The scattering diagram is a simple two-axis plot of intensity versus angle. In other words, the scattering diagram shows the scattered intensity at a point some exact angle from the axis. There are plots in Appendix B for fiber diameters of each whole micrometer between one and twenty. Designing with data for the entire range ensures that the requirements are met for the desired diameter coverage and linearity of response.

4.3 CALCULATION OF THE TOTAL POWER SCATTERED INTO A REGION

Although an optical system using a photo-detector actually responds to the total power incident on the detector, it is sufficient to use the average intensity in some region as the design parameter. The goal of the design is the determination of the required region of space such that power incident on the detector has a linear relationship with fiber diameter. For some regions of space, the relationship between total scattered power and fiber diameter may be not only non-linear, but also non-monotonic. This effect is usually noticed when using very small diameter fibers and measuring total power scattered into angles near zero. As either the fiber diameter or the angle increases, the relationship becomes more monotonic. Once some region has been defined, the total power scattered into said region is simply the average intensity in the region multiplied by the area contained in the region. It is easily seen that if the area is held to be constant, the average intensity is perfectly correlated with the total power. Therefore, if the design goal is modified to be the determination of the required region of

space such that the average intensity throughout the region has a linear relationship with fiber diameter, the primary goal involving total power is automatically satisfied.

4.4 LINEARITY OF THE RESPONSE FUNCTION

After extensive work with the results of the calculations of Chapters 2 and 3, it has been found that the region of space with the optimum relationship with fiber diameter is twenty degrees wide and centered at forty degrees from the axis. Figure 3 shows a plot of the average intensity in this region versus fiber diameter. Using a least-squares method of curve fitting yields the following linear relationship

$$I = 6.1 \times 10^{-4} + (0.0063)(\text{diameter of fiber}) \qquad (4.1)$$

where the diameter is expressed in micrometers. The coefficient of correlation calculated by a least squares linear best fit method between the data presented in Table I and plotted in Figure 3 and the data represented by the straight line in equation (4.1) has the value of

$$R = 0.9979 \qquad (4.2)$$

The intensity as calculated by (4.1) may be considered to be a normalized intensity, as it was generated assuming a unit intensity incident upon the fiber.

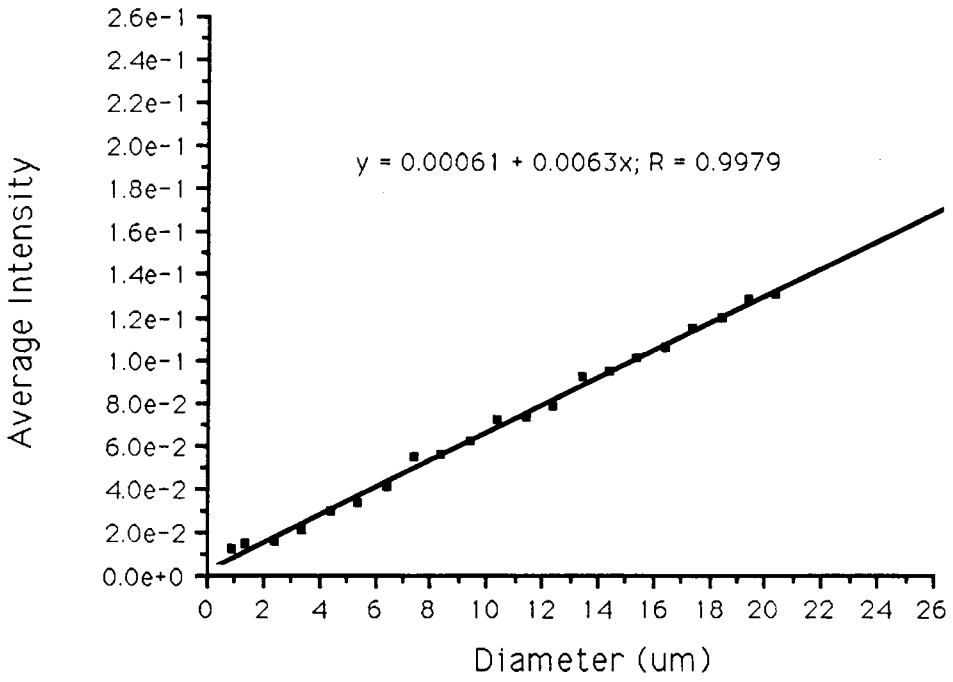


Figure 3. Theoretical Average Intensity Over the 30 to 50 Degree Range Versus Cylinder Diameter in Micrometers

TABLE I

Theoretical Average Intensity Over the 30°-50° Range For Various Cylinder Diameters

D (um)	Intensity (W/m^2)
1	0.00985
2	0.01152
3	0.01628
4	0.02509
5	0.02899
6	0.03571
7	0.05029
8	0.05116
9	0.05667
10	0.06721
11	0.06844
12	0.07367
13	0.08682
14	0.08961
15	0.09611
16	0.10074
17	0.10923
18	0.11493
19	0.12265
20	0.12529

CHAPTER V

DESIGN OF THE OPTICAL SENSOR BASED ON THEORETICAL RESULTS

5.1 DESIGN CONSTRAINTS

Based on the results of the above calculations, a new optical sensing unit must be designed and implemented. The fundamental constraint is that the sensor must provide for the collection and measurement of all radiation scattered between the angles of 30 and 50 degrees from the direction of propagation by the glass fiber in transit through a generated beam of light. A mechanical constraint that must be imposed is that the optics must be capable of making the measurement of fibers that pass through different portions of the sampling volume. For mechanical reasons relating to the total airflow through the sensor, the required field of view is a circular area of diameter five millimeters.

5.2 GENERATION OF THE PLANAR WAVEFRONT

Since it is known that the fibers are supported in an air stream as they transit the sensor, it is desirable to generate a beam of light which adequately covers an entire cross-section of the air flow. This is necessary to ensure that all fibers present in the air flow are presented for measurement. Referring to Figure 2, the y-dimension of the beam must be at least five millimeters. To assure a uniform intensity and subsequently a uniform measurement across this area, the beam actually generated is eight millimeters wide.

To facilitate measurement of the cylinder diameter at different points along the length of the fiber rather than the average diameter across large portions of the length, the generated light beam must be very narrow in the z-dimension (Fig. 2). The diffraction limit for non-polarized near-infra-red radiation is

approximately five-hundred microns. By focusing the beam to this dimension at the point of measurement, the mean diameter of the fiber along a five-hundred micron section of the length may be measured.

The optical system selected for the generation of the propagating wavefront is shown in Fig. 4. The source is a light emitting diode made by Motorola which yields five milliwatts of optical power. A search was made to find the highest power LED available since the strength of the resulting signal depends directly on the intensity of the beam. This particular source emits the majority of its power in a narrow range of angles from its axis as shown by the manufacturer's data in Fig. 5. As the active area of the diode is only forty micrometers in diameter, the LED may be considered to a good approximation to be a point source of radiation.

The thirty millimeter focal length achromatic lens is placed relative to the LED as shown (Fig. 4) so that the light collected from the source is focussed in a conical shape reaching a point somewhere on the other side of the sampling volume. The shape of the cone must be such that the diameter of a cross-section taken at the sampling volume is eight millimeters. This ensures that the beam is at least the minimum width.

A cylindrical lens with a eighty millimeter focal length is placed immediately following the achromat. This lens allows the beam to pass completely undisturbed in the y-dimension while acting to bring it to a sharp focus at the sampling volume in the z-dimension. The sampling volume is a circular region in the x-y plane surrounding the z-axis. Figures 6a and 6b illustrate the effects of the cylindrical lens by showing the outline of the propagating wave in both dimensions.

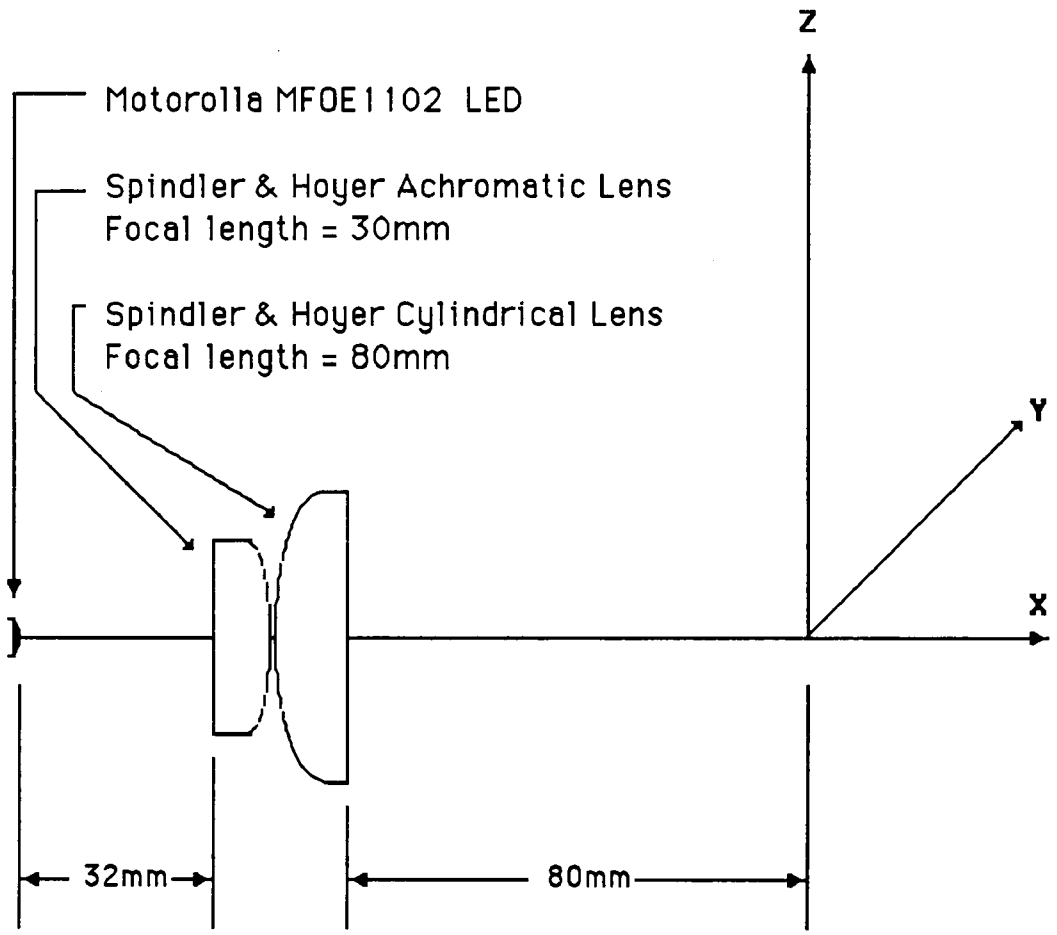


Figure 4. Optical Arrangement for the Generation of the Propagating Wave

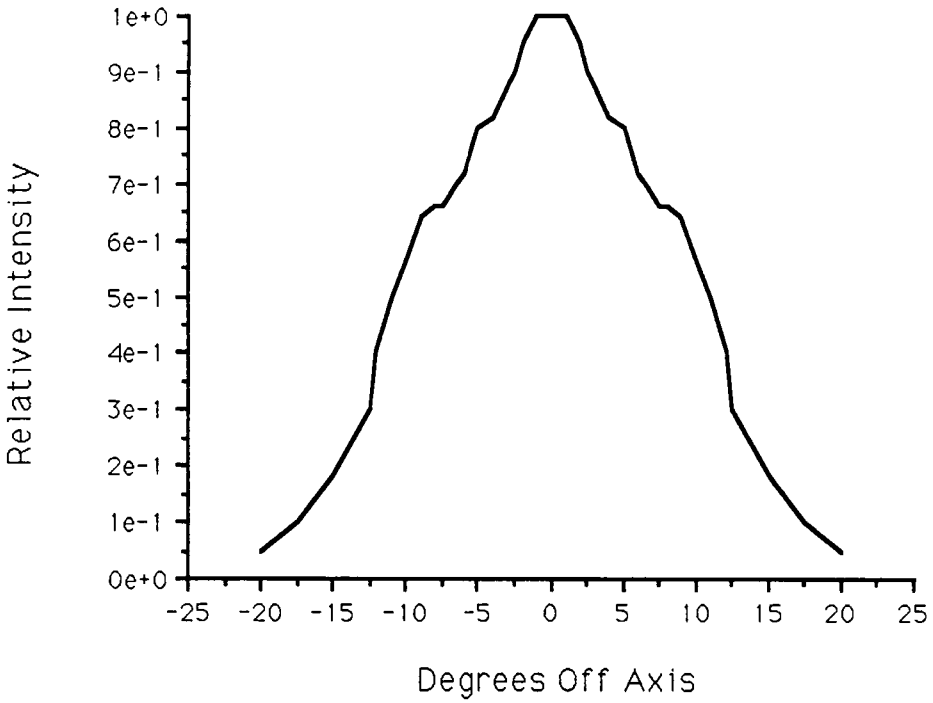
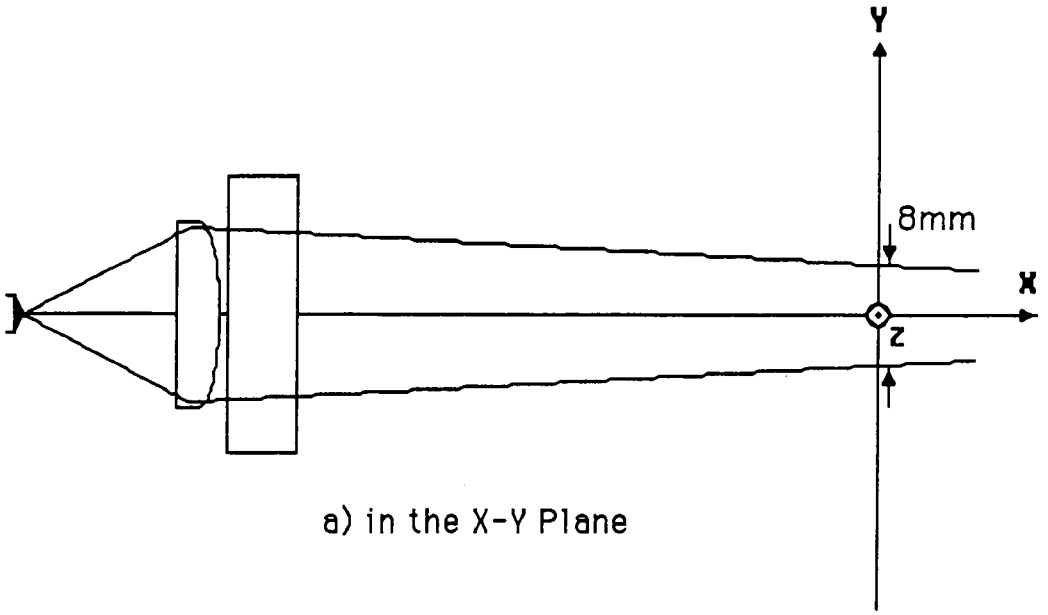
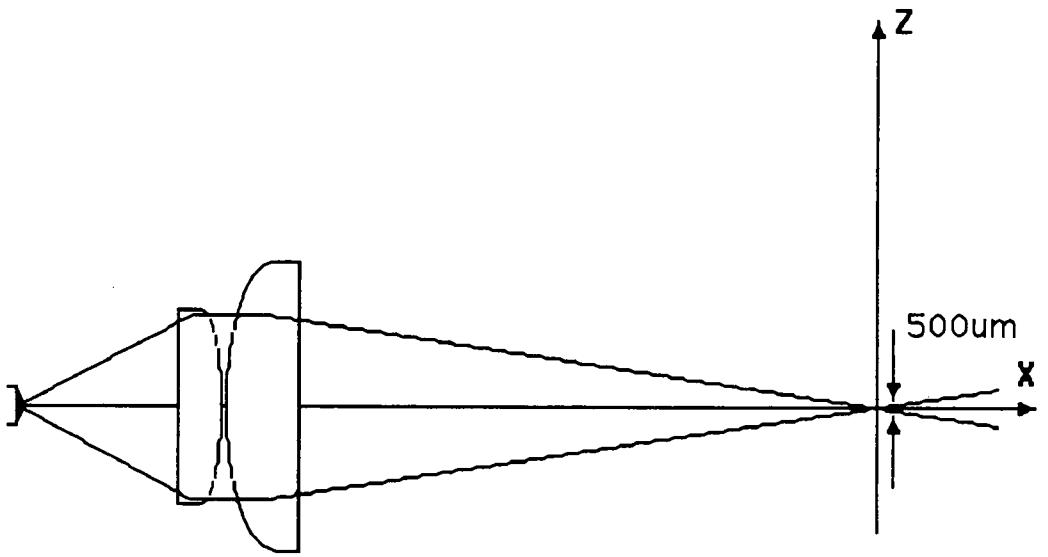


Figure 5. Radiation Pattern of the Motorola Diode



a) in the X-Y Plane



b) and in the X-Z Plane

Figure 6. Ray Approximation to the Propagating Plane Wave

The thickness of the beam in the z-dimension at the focal point of the cylindrical lens is determined by the diffraction limit. Equation (5.1), taken from [8], is used to calculate the actual thickness as being 486 micrometers.

$$W = \frac{4f\lambda}{\pi m W_1}\sqrt{1 + \frac{(4f\lambda)^2}{(\pi m W_1)}} \qquad (5.1)$$

The actual spot-size, W, at the focal point is a function of the focal length of the lens, f, the wavelength of the light, λ, the index of refraction of the medium, m, and the original spot-size incident on the lens, W_1. From (5.1) it is obvious that shorter focal length lenses yield smaller spot sizes as does shorter wavelength light.

5.3 MEASUREMENT OF THE TOTAL POWER SCATTERED INTO THE REGION OF INTEREST

The region of interest as determined in Chapter 4 lies between 30 and 50 degrees from the axis of propagation. Therefore, it is necessary to block any and all light that does not originate from the vicinity of the fiber and that does not fall within this region. Figure 7 illustrates the optical system chosen for the collection of the scattered power. In order to collect light out to fifty degrees, a Fresnel lens with a clear aperture of 33 millimeters must be placed 14 millimeters from the fiber. Because of the circular symmetry of the lens, light emanating from a point at the center of the sampling volume and making an angle of fifty degrees with the x-axis in any plane is collected by the lens. This illustrates that the scattering on both sides of the x-axis is collected, thus doubling the signal power. In order to prevent the propagating wave as well as the scattering at angles smaller than 30 degrees from being collected, it is necessary to place a 16 millimeter diameter beam-dump in the center of the Fresnel lens as shown in Fig. 7. The beam-dump is

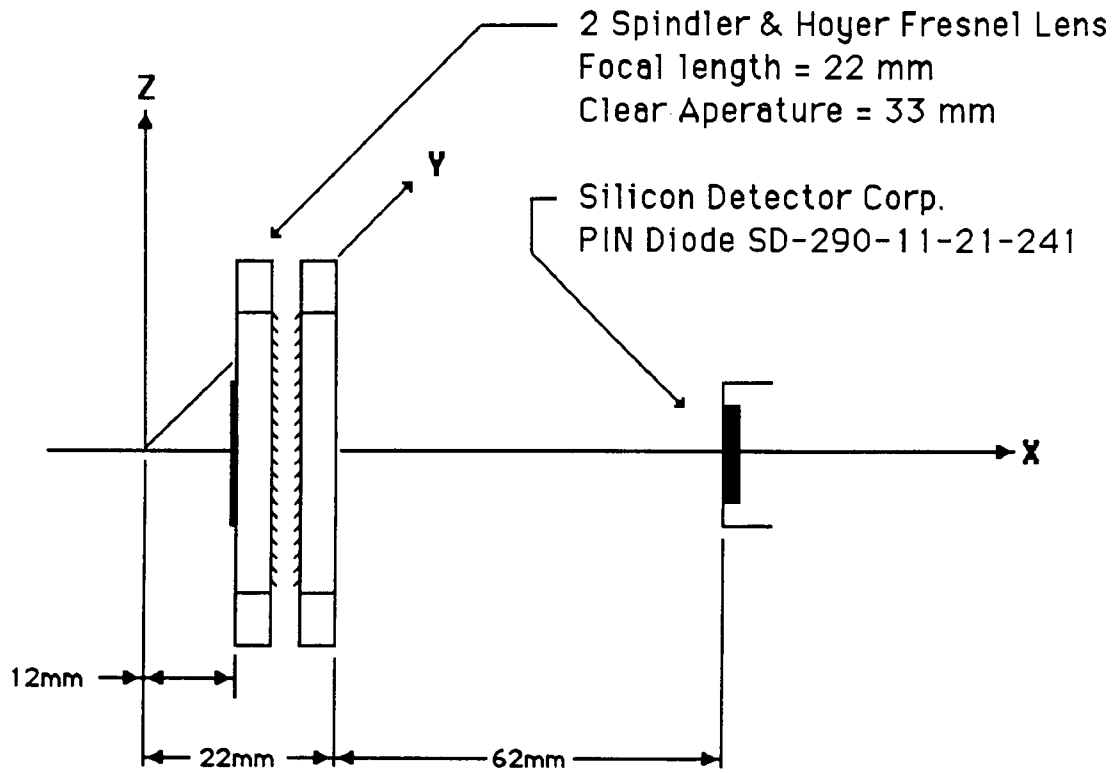


Figure 7. Optical Arrangement for the Collection of Scattered Power

simply a black anodized aluminum disc which will absorb any light incident upon it.

In order for the Fresnel lens to be able to focus the collected light onto the photo-detector, its focal length must be somewhat less than the 14 millimeter distance to the fiber. Unfortunately, the minimum focal length currently available in a lens with the required diameter is 12 millimeters. While this would suffice to focus the collected light onto the detector, it would require the detector to be a rather large distance from the lens, thereby increasing the physical size of the sensing unit. The addition of the second Fresnel lens as shown in Fig. 7 creates a much shorter effective focal length and allows the detector to be relatively close to the lens.

5.4 ANALOG SIGNAL PROCESSING

Based on the results of Chapter 4, the minimum probable signal is approximately 10 nW of optical power. A total system gain of 25×10^6 V/W will produce a signal of 250 mV. Since the responsivity of most all PIN diode-type detectors is 0.5 A/W, a transimpedance gain of 50×10^6 V/A is required. A bandwidth of 1 MHz is required in order to adequately reproduce the shape of the leading and trailing edges of the current pulses. Although much higher bandwidth as well as a lower noise level could be obtained using discrete design techniques, a simple operational amplifier circuit was chosen. The circuit of Figure 8 was selected for its simplicity and reasonable performance. The single most troublesome feature of the circuit is the relatively high capacitance of the detector itself. The manufacturer's data indicates that it is approximately 100 pF. This capacitance necessarily interacts with the input to a current sensitive amplifier and can greatly reduce the bandwidth of the system as well as influence the circuit's stability against oscillation.

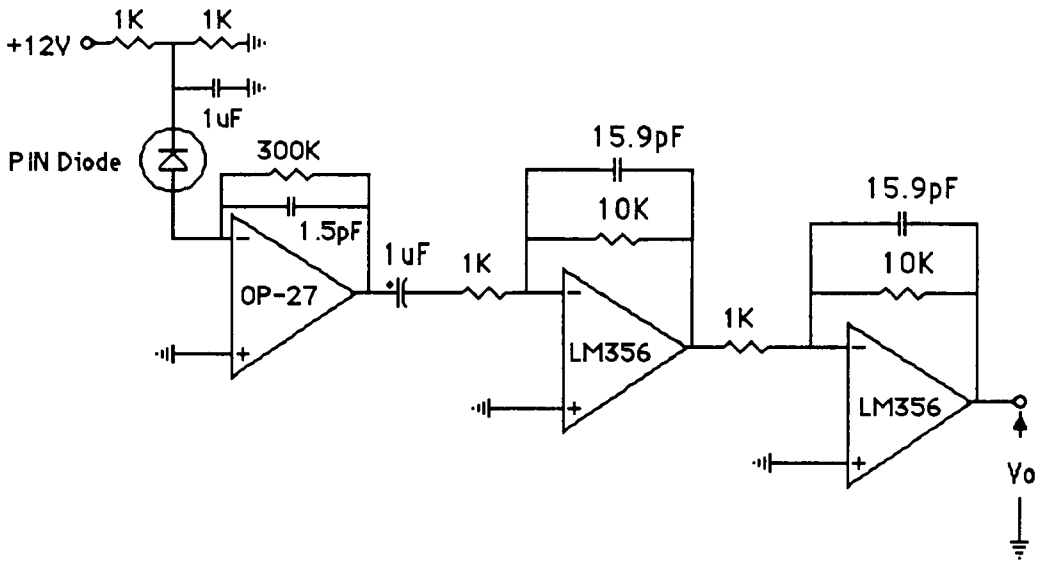


Figure 8. Basic Circuit for the Analog Signal Processing

CHAPTER VI

EXPERIMENTAL RESULTS

6.1 TEST CIRCUITRY

For the purposes of verifying the response function of the sensor, it was decided to use a static test rather than attempt to pass the fibers through the sensor in an airstream. Placing the fibers in the sampling volume manually allows a much greater degree of control in the measurement process and eliminates many possible sources of error. Since the fibers are at rest within the sensor, the AC-coupled circuitry for production in Figure 8 will not be satisfactory for the static tests. Therefore a simple low-pass system with the same gain as in Figure 8 was developed. This circuit is illustrated in Figure 9.

6.2 FIBER PREPARATION

In order to manipulate a large number of micrometer size fibers without damage, a method was arranged to allow each fiber to be permanently attached to a small wooden handle. These handles were then clamped in a micro-manipulator which provided a fine control over the position of the fiber in the sensor. A total of 22 fibers ranging in size from 23.5 down to 1.5 micrometers were prepared in this way. Those fibers at the large end of the size range were relatively easy to prepare. However, the smaller fibers required the use of a sharpened tungsten needle to manipulate onto the handles. Fibers with diameters below about 4 micrometers are not visible to the naked eye.

Each fiber, once attached to a handle, was measured under a microscope using a magnification of 1000x and a reticule which was scaled in 1 micrometer increments at that magnification.

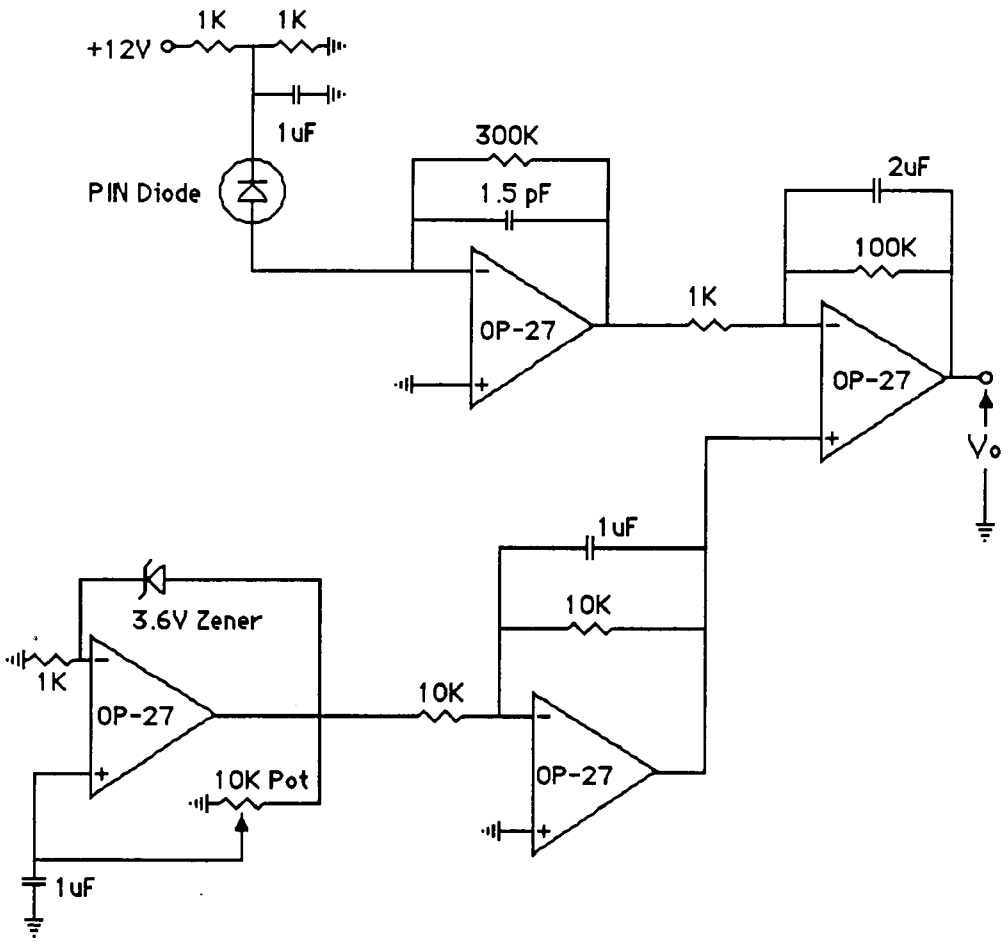


Figure 9. Directly Coupled Circuit for Static Testing

6.3 CORRELATION OF THE RESULTS WITH THEORY

Each of the prepared fibers was positioned in the sensor at the center of the sampling volume. Some effort was expended to ensure that each fiber would be placed at the same location by monitoring the measurements of the micrometers built into the micro-manipulator in order to avoid variations in the measurements due to position. The signal was taken to be the DC voltage difference between the conditions with and without a fiber present. A voltage level measurement was made both before positioning the fiber and after removing the fiber to verify that there had been no significant drift in the electronics or variation in any of the rest of the experimental setup in the course of making the measurement. Table II contains the diameters of the fibers as measured under the microscope as well as the DC voltage measurement for each. Figure 10 is a graphic illustration of this data. Using the same least-squares method of curve fitting as in section 4.4 produces the linear relationship between incident power and fiber diameter given in (6.1).

$$I = 1.9 \times 10^{-3} + (0.0061)(\text{diameter of fiber}) \qquad (6.1)$$

The correlation coefficient between the straight line (6.1) and the data in Table II was found to be

$$R = 0.9977 \qquad (6.2)$$

This relationship agrees very well with the predicted relationship between incident power and fiber diameter. With this very linear relationship, obviously, a very good prediction of diameter can be made based on a known output voltage.

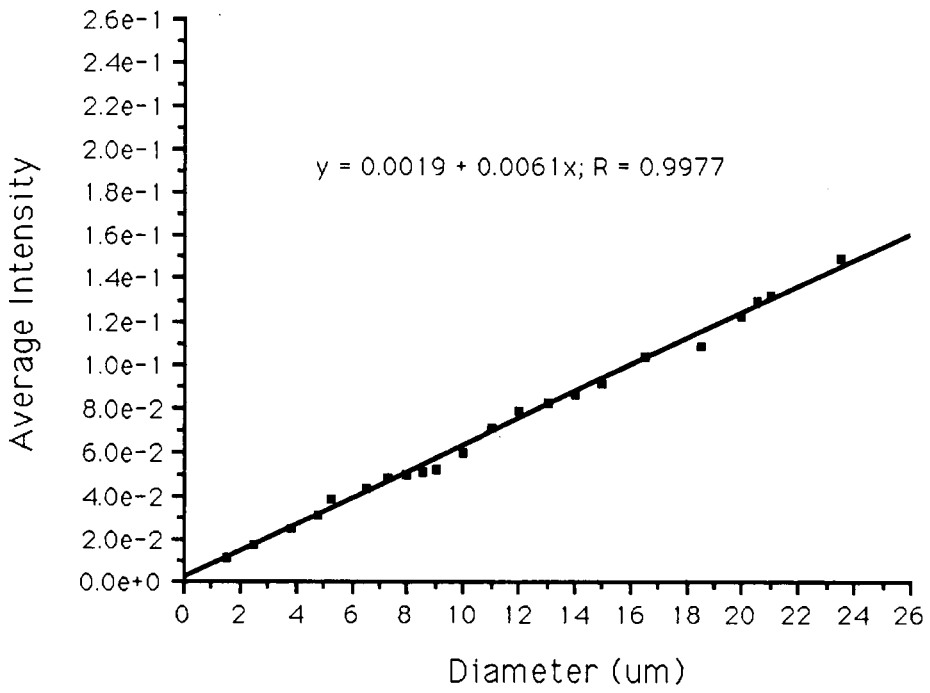


Figure 10. Experimental Average Intensity Over the 30 to 50 Degree Range Versus Cylinder Diameter in Micrometers

TABLE II

Experimental Output Voltage and Corresponding Average Intensity From the 30°-50° Range For Various Cylinder Diameters

D (um)	Volts	Intensity (W/m^2)
1.5	0.43	0.01123
2.5	0.67	0.01749
3.8	0.95	0.02480
4.8	1.19	0.03107
5.3	1.48	0.03864
6.5	1.67	0.04360
7.3	1.84	0.04803
8.0	1.90	0.04960
8.5	1.97	0.05143
9.0	2.01	0.05247
10.0	2.30	0.06004
11.0	2.70	0.07048
12.0	3.00	0.07832
13.0	3.15	0.08223
14.0	3.29	0.08589
15.0	3.50	0.09137
16.5	3.95	0.10312
18.5	4.15	0.10834
20.0	4.67	0.12191
20.5	4.95	0.12922
21.0	5.04	0.13157
23.5	5.73	0.14958

CHAPTER VII

CONCLUSION

7.1 GENERAL SUMMARY

The primary goal of this thesis was to present as a design aid methods of computing the exact theoretical solution of the scattering of electromagnetic radiation. The fundamental problem is the design of optical instrumentation capable of fast, non-contact measurement of the diameter of particles. Previously, this field involved largely intuitive design work based on a thorough understanding of the theoretical background and the dominant effects. While no degree of exactness in the calculation of expected results will ever be a substitute for a thorough understanding of the problem, algorithms developed for this thesis will allow the experienced designer to more readily verify that the design will yield useful performance.

7.2 AREAS FOR FURTHER STUDY

One serious limitation to the process so far developed is its restriction to real indices of refraction. By far, most substances have complex indices. The imaginary portion of the index of refraction relates to the absorption of light by the substance. A useful addition to the method would be the capability for designing to measure particle or fiber sizes of these substances.

Another short-coming of the design software as it now exists is the limited information provided as output. A useful addition would be the capability of specifying a region over which the total power should be calculated. Convergence algorithms designed to iterate to a selection of the most linear region should be fairly straight-forward to implement and would be of great benefit.

LIST OF REFERENCES

LIST OF REFERENCES

1. Lord Rayleigh, Philos. Mag. 12, 81 (1881).

2. J. L. Lundberg, "Light Scattering From Large Fibers at Normal Incidence," Journal of Colloid and Interface Science, 29, 3, pp. 565-582 (1969).

3. M. Born and E. Wolf, Principals of Optics, (Pergamon Press, New York, 1964).

4. M. Abramowitz and I. A. Stegun, Handbook of Mathematical Functions, (Dover, New York, 1965).

5. H. C. van de Hulst, Light Scattering by Small Particles, (Dover, New York, 1957).

6. M. Kerker, The Scattering of Light and Other Electromagnetic Radiation, (Academic Press, New York, 1969).

7. M. Kerker and W. A. Farone, Journal of the Optical Society of America, 56, 481 (1966).

8. A. Yarriv, Optical Electronics, (Holt, Rinehart and Winston, New York, 1985).

APPENDICES

APPENDIX A

This appendix contains the code for the pascal program used to generate the scattering plots. There are six main subroutines used by the program. The first, called SCREEN, handles all of the screen controls to query the user for the necessary physical parameters as well as the range over which to generate the scattering plot. COMPUTE_BESSELS, the second procedure used by the main program, is responsible for the computation of the Bessel functions, the Neumann functions, and their derivatives for the given argument of all orders up to the upper limit. The argument and upper limit must be passed to the routine. The Bessel functions of the first kind are computed using the method of Abramowitz and Stegun as discussed in section 3.3 of this thesis. The Neumann functions are computed using the polynomial approximations for the low orders and then the forward recursion for higher orders. The derivatives are obtained directly using the relationships previously discussed. The procedure COMPUTE_ARRAYS is responsible for determining which arguments are to be used in the computation of the Bessel functions and what the upper limits should be. COMPUTE_ARRAYS then uses COMPUTE_BESSELS to generate the required results for each of the necessary arguments. Finally, COMPUTE_ARRAYS uses the expressions given by (2.37) and (2.38) to generate the so-called Mie coefficients. The procedure COMPUTE_SUMS utilizes these Mie coefficients and handles the complex arithmetic to implement the summations in equation (2.39) for some given angle Θ. COMPUTE_INTENSITY uses the results from COMPUTE_SUMS to calculate the actual intensity at a point in space defined by the angle Θ and the radius r. The main program loop cycles through a loop designed to compute the intensities at the radius selected by the user at one-tenth degree intervals within the degree range also selected by the user. The procedure POWER uses the rectangular approximation to take the integral of the intensity across one-degree spans within the range of interest. The result is that the

average optical power scattered into a region of space defined by some radius **r** and range of angles $\Theta \pm$ one-half degree is known. At present, these results are echoed on the monitor as each degree range is computed and then stored in an ASCII file in permanent storage at the end of the program. No effort is made to generate actual plots within the program at this time, although that would be a useful addition.

```
program scatter (input,output,data);

const
    PI = 3.14159265;
type
    Parray      = Array [1..90] of real;
    Iarray      = Array [1..1000] of real;
    Holder      = Array [0..500] of real;
    Complex     = record
        Re  : real;
        Im  : real;
        end; {record definition}
    Elements = Array [0..1000] of Complex;
    { Type ELEMENTS is used to hold up to1000 complex numbers }
var
    Data        : TEXT;     { Output file }
    D           : real;     { Cylinder diameter (um) }
    M           : real;     { Refractive index }
    Intn        : real;     { Incident intensity }
    R           : real;     { Observation distance }
    Degree      : real;     { Current angle of loop }
    Lambda      : real;     { Incident wavelength }
    Start_angle : real;     { Beginning and end of }
    End_angle   : real;     {  user selected range }
    Sum         : real;
    Sumlimit    : integer;
    Index       : integer;
    Inc         : integer;
    Intensity   : Iarray;
    Av_Power    : Parray;
    An          : Elements; { Arrays for holding Mie }
    Bn          : Elements; {  coefficients }
    Asum        : Complex;  { Arrays for summations }
    Bsum        : Complex;  {  of An and Bn }
```

```
procedure Screen (   var d              : real;
                     var m              : real;
                     var Intn           : real;
                     var r              : real;
                     var Lambda         : real;
                     var Start_angle    : real;
                     var End_angle      : real );
begin
     Clrscr;
     TextColor(White);
     d := 1;
     write('Fiber diameter (um) ?      (Default = 1) ');
     readln (d);
     m := 1.5;
     write('Refractive index ?       (Default = 1.5) ');
     readln (m);
     Intn := 1;
     write('Beam intensity ?          (Default = 1) ');
     readln (Intn);
     r := 45;
     write('Observation distance (mm)?  (Default = 45) ');
     readln (r);
     Lambda := 0.84;
     write('Wavelength (um) ?    (Default = 0.84, NIR) ');
     readln (Lambda);
     Start_angle := 0.1;
     write('Smallest angle (degrees)? (Default = 0.1 ) ');
     readln(Start_angle);
     End_angle := 90;
     write('Largest angle (degrees)?  (Default = 90 ) ');
     readln(End_angle);
end; {procedure Screen}
```

```
procedure Compute_Bessels ( var Jarray   : Holder;
                            var dJarray  : Holder;
                            var Yarray   : Holder;
                            var dYarray  : Holder;
                                arg      : real;
                                limit    : integer );
var
    Index : integer;
    Sum   : real;

begin
    Jarray [limit] := 0;
    Jarray [limit-1] := 1;
    For index := limit-2 downto 0 do
        Jarray[index]:=2*(index+1)/arg*Jarray[index+1] +
                       Jarray[index+2];
    sum := Jarray[0];
    For index := 1 to trunc(limit/2+0.5) do
        sum := sum + 2*Jarray[2*index];
    For index := 0 to limit do
        Jarray[index] := Jarray[index]/sum;


    if (Abs(arg) <= 3) then
    Yarray[0] :=  2/PI*LN(arg/2)*Jarray[0] + 0.36746691
                  + 0.60559366*sqr(arg)/9
                  -0.74350384/81*sqr(arg)*sqr(arg)
                  + 0.25300117/729*sqr(sqr(arg))*sqr(arg)
                  -0.04261214/729/9*sqr(sqr(sqr(arg)))
                  + 0.00427916/729/81*sqr(sqr(sqr(arg)))
                      *sqr(arg)
                  -0.00024846/729/729*sqr(sqr(sqr(arg)))
                      *sqr(sqr(arg))
    else
```

```
    Yarray[0] :=  (0.79788456 - 0.00000077*3/arg
                  -0.0055274*9/sqr(arg)
                  -0.00009512*27/sqr(arg)/arg
                  + 0.00137237*81/sqr(sqr(arg))
                  -0.00072805*243/sqr(sqr(arg))/arg
                  + 0.00014476*729/sqr(sqr(arg))
                       /sqr(arg))/sqrt(arg)
                       * sin(arg - 0.78539816
                  -0.014166397*3/arg
                  -0.00003954*9/sqr(arg)
                  + 0.00262573*27/sqr(arg)/arg
                  -0.00054125*81/sqr(sqr(arg))
                  -0.00029333*243/sqr(sqr(arg))/arg
                  + 0.00013558*729/sqr(sqr(arg))/sqr(arg));

    Yarray[1] := (Jarray[1]*Yarray[0] - 2/PI/arg)/Jarray[0];
    For index := 2 to limit do
        Yarray[index] :=  2*(index-1)/arg*Yarray[index-1]
                          - Yarray[index-2];

    dJarray[0] := - Jarray[1];
    For index := 1 to limit do
        dJarray[index] := Jarray[index-1] -
                          index/arg*Jarray[index];
    dYarray[0] := - Yarray[1];
    For index := 1 to limit do
        dYarray[index] := Yarray[index-1]
                          - index/arg*Yarray[index]

end; { Procedure Compute_Bessels }
```

```
procedure Compute_Arrays ( var An          : Elements;
                           var Bn          : Elements;
                           var Sumlimit    : integer;
                               d           : real;
                               lambda      : real;
                               m           : real );
var
    Index, limit      : integer;
    L, Q, N, P, Alpha : real;
    Jalpha, Jalpham, Yalpha, Yalpham     : Holder;
    dJalpha, dJalpham, dYalpha, dYalpham : Holder;
begin
    Alpha := PI * d / Lambda;
    limit := Trunc(10*sqrt(m*Alpha)+4.5);
    sumlimit := limit - 2;

Compute_Bessels (  Jalpha, dJalpha, Yalpha, dYalpha,
                   Alpha,  limit);
Compute_Bessels (  Jalpham, dJalpham, Yalpham, dYalpham,
                   Alpha*m, limit);
For index := sumlimit downto 0 do
begin
    L := Jalpha[index] * dJalpham[index]
         - m * dJalpha[index] * Jalpham[index];
    Q := Yalpha[index]*dJalpham[index]
         - m * dYalpha[index] * Jalpham[index];
    N := m * Jalpha[index] * dJalpham[index]
         - dJalpha[index] * Jalpham[index];
    P := m * Yalpha[index] * dJalpham[index]
         - dYalpha[index] * Jalpham[index];

if L = 0 then
    An [index].Re := 0
else if ( abs(L) <= 1E-15 * abs(Q) ) then
```

```
            An[index].Re := L/Q
else An[index].Re := 1 / ( 1 + sqr(Q/L) );

if ( abs(L)<1E-15 ) AND ( abs(Q)<1E-15 ) then
begin
     L := L/1E-15;
     Q := Q/1E-15;
     An[index].Im := ( L*Q ) / ( sqr(L)+sqr(Q) )
end
else An [index].Im := ( L*Q )/( sqr(L)+sqr(Q) );

if N = 0 then
     Bn [index].Re := 0
else if ( abs(N) <= 1E-15 * abs(P) ) then
          Bn[index].Re := N/P
else Bn[index].Re := 1 / ( 1 + sqr(P/N) );

if ( abs(N)<1E-15 ) AND ( abs(P)<1E-15 ) then
begin
     N := N/1E-15;
     P := P/1E-15;
     Bn[index].Im := N*P / ( sqr(N)+sqr(P) )
end
else Bn [index].Im := N*P / ( sqr(N)+sqr(P) )
end; { procedure  Compute_Arrays }
```

```
procedure Compute_Sums (    var  ASum       : Complex;
                            var  BSum       : Complex;
                                 An         : Elements;
                                 Bn         : Elements;
                                 degree     : real;
                                 sumlimit   : integer );
var
    Index    : Integer;
    Temp     : Complex;
    Theta    : Real;
begin
    Asum.re      := An[0].re;
    Asum.im      := An[0].im;
    Bsum.re      := Bn[0].re;
    Bsum.im      := Bn[0].im;
    Theta        := degree * 2 * PI / 360;
    For Index := 1 to Sumlimit do
    begin
        Asum.re :=   Asum.re + An[index].re * 2
                     * cos(Index * Theta);
        Asum.im :=   Asum.im + An[index].im * 2
                     * cos(Index * Theta);
        Bsum.re :=   Bsum.re + Bn[index].re * 2
                     * cos(Index * Theta);
        Bsum.im :=   Bsum.im + Bn[index].im * 2
                     * cos(Index * Theta)
    end;
    Temp     := Asum ;
    Asum.re  := sqr(temp.re) - sqr(temp.im);
    Asum.im := 2 * temp.re * temp.im;
    Temp := Bsum ;
    Bsum.re := sqr(temp.re) - sqr(temp.im);
    Bsum.im := 2 * temp.re * temp.im
end; { procedure Compute_Sums }
```

```
procedure Compute_Intensity (var    Intensity : real;
                                    Asum      : Complex;
                                    Bsum      : Complex;
                                    Intn      : real;
                                    Lambda    : real;
                                    r         : real );
var
    Temp : Complex;
begin
    Temp.re      := asum.re + bsum.re;
    Temp.im      := asum.im + bsum.im;
    Intensity    := Intn * Lambda/sqr(PI)/r/2 *
                    sqrt(sqr(temp.re) + sqr(temp.im))
end; { procedure Compute_Intensity }
```

```
procedure Power (var     data        : Text;
                         d           : real;
                 var     Av_Power    : PArray;
                         Intensity   : IArray );
var
    sum : real;
    inc  : integer;
begin
    Assign (data,'data'+CHR(Round(d) DIV 10 + 48)
            +CHR(Round(d) MOD 10+48)+'.pwr');
    Rewrite(data);
    writeln(data);
    writeln(data,'    Average intensity per degree range
            taken from 1/10 degree samples.');
    writeln(data,'    Fiber diameter = ',d:4:1);
    writeln(data);
    For Index := 1 to 90 do
    begin
        sum := 0;
        For inc := (10*index-9) to (10*index) do
            sum := sum + 0.1*Intensity[inc];
        Av_Power[index] := sum;
        write(data,index-1:2,' to ',index:2,
                ' degrees, Average = ',sum:7:4,'  ');
        if (index MOD 2 = 0) then writeln(data)
    end;
    Flush(data)
end; { procedure Power }
```

```
{ Main Routine }
begin

Screen (d,m,Intn,r,Lambda,Start_angle,End_angle);
Compute_Arrays ( An, Bn, sumlimit, d, Lambda, m );
For Index := 1 to 900 do
     Intensity[index] := 0;
For Index := Round(10*Start_angle) to Round(10*End_angle) do
begin
     degree := Index/10;
     write ('degree = ',degree:4:4);
     Compute_Sums ( Asum, Bsum, An, Bn, degree, sumlimit );
     Compute_Intensity (  Intensity[index], Asum, Bsum, Intn,
                          Lambda, r );
     writeln('     I = ',Intensity[index]:4:4)
end;
Power (data,d,av_power,intensity)
end.
```

APPENDIX B

This appendix contains the scattering diagrams generated by the program in Appendix A for glass cylinders scattering light of 840 nm wavelength. The index of refraction is taken to be 1.5 exactly and the cylinders range in diameter from one to 20 micrometers. The incident intensity and observation distance are taken arbitrarily to be one watt and one meter, respectively.

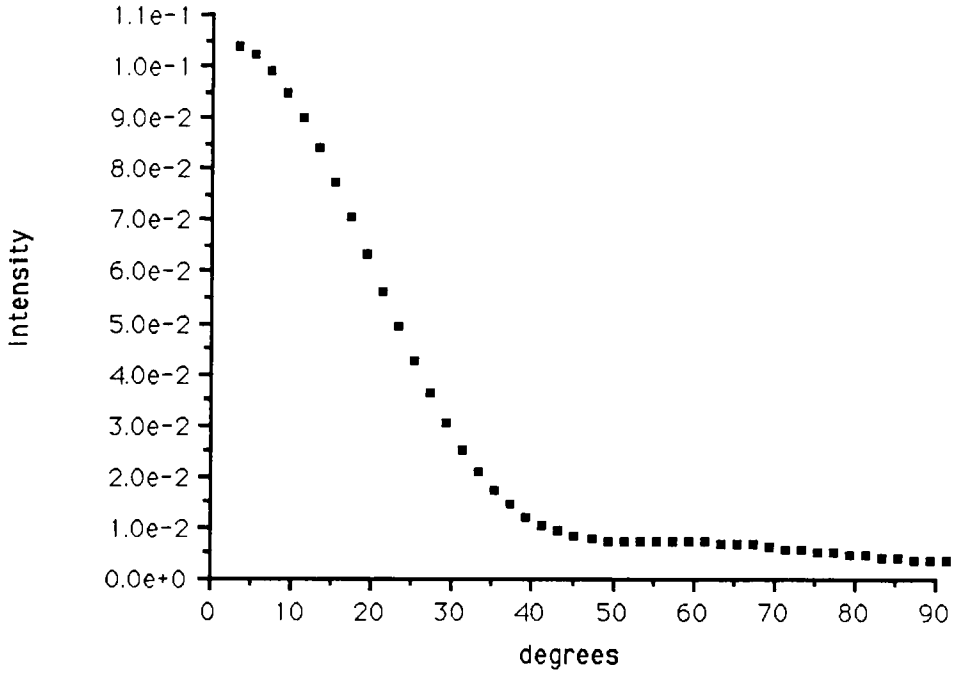


Figure 11. Theoretical Plot of Intensity Versus Angle for Glass Cylinders of 1 Micrometer Diameter

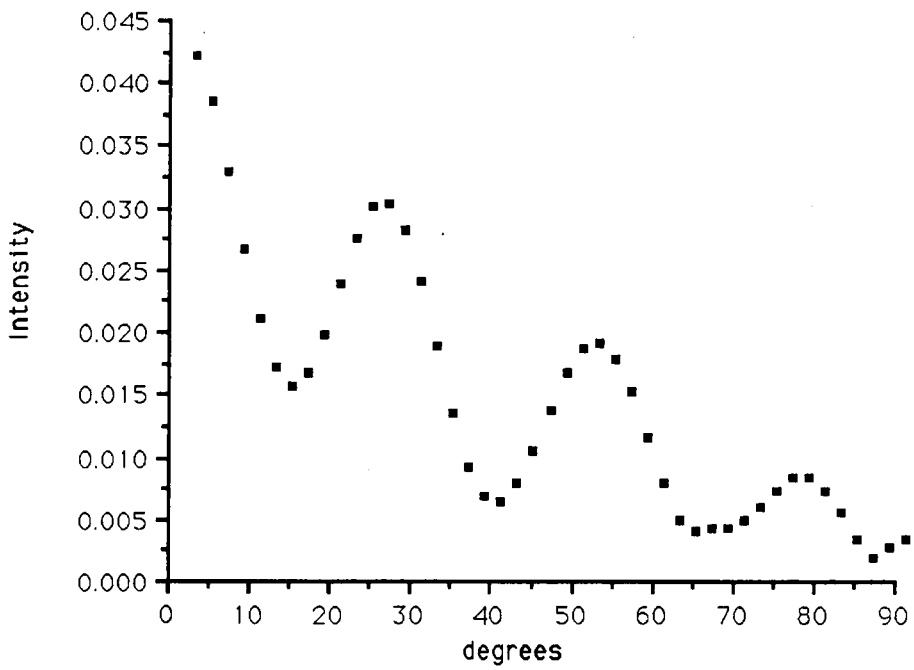


Figure 12. Theoretical Plot of Intensity Versus Angle for Glass Cylinders of 2 Micrometer Diameter

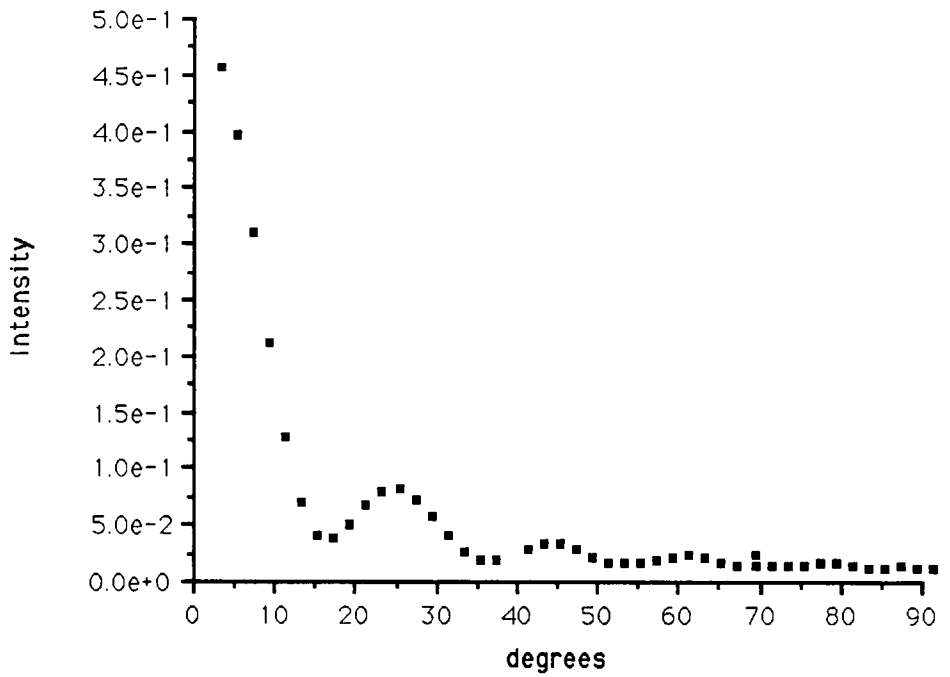


Figure 13. Theoretical Plot of Intensity Versus Angle for Glass Cylinders of 3 Micrometer Diameter

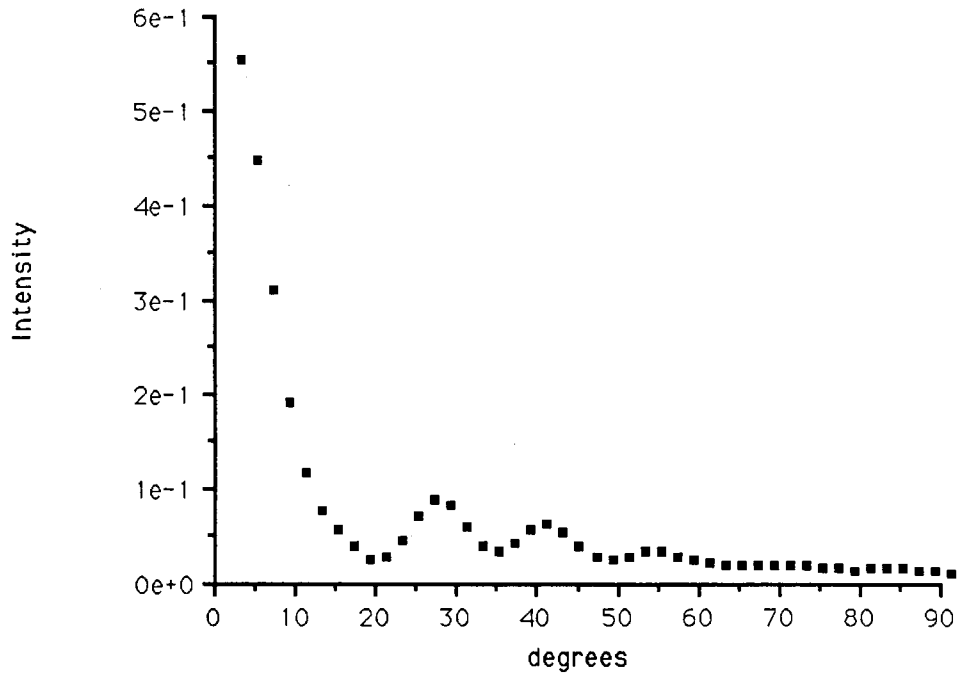


Figure 14. Theoretical Plot of Intensity Versus Angle for Glass Cylinders of 4 Micrometer Diameter

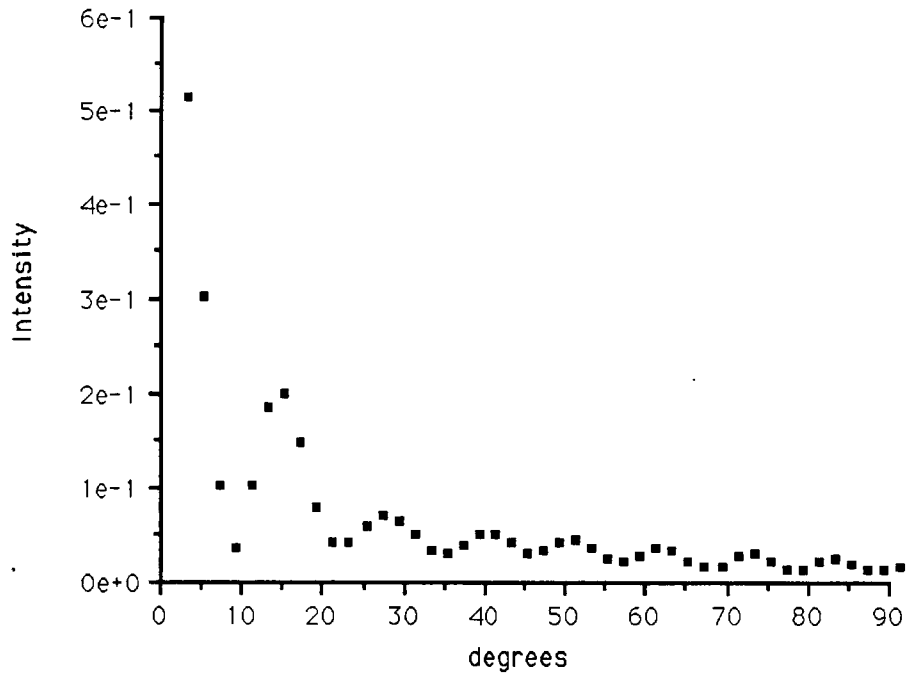


Figure 15. Theoretical Plot of Intensity Versus Angle for Glass Cylinders of 5 Micrometer Diameter

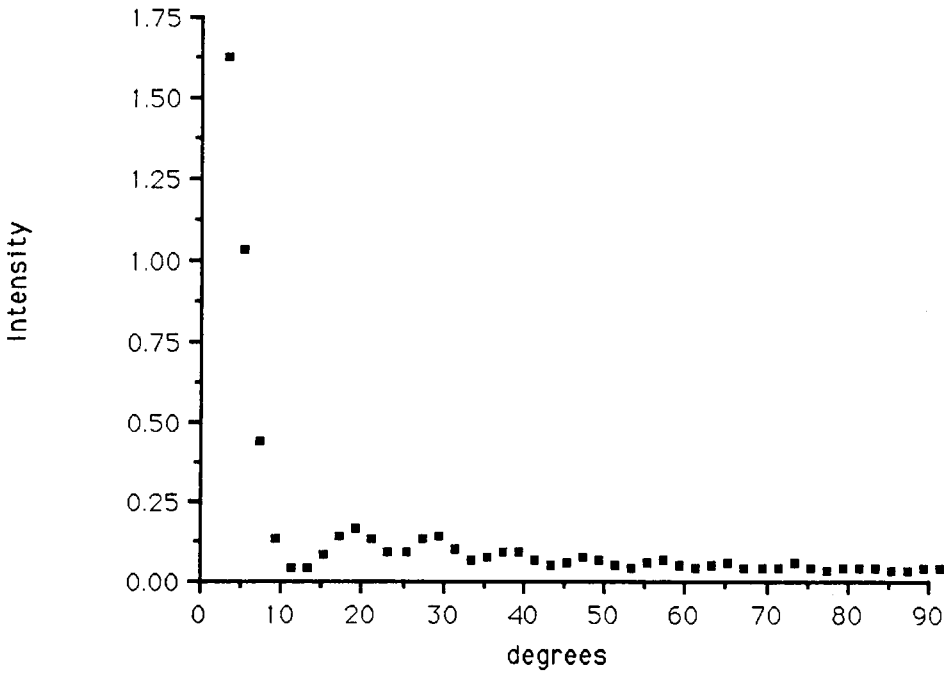


Figure 16. Theoretical Plot of Intensity Versus Angle for Glass Cylinders of 6 Micrometer Diameter

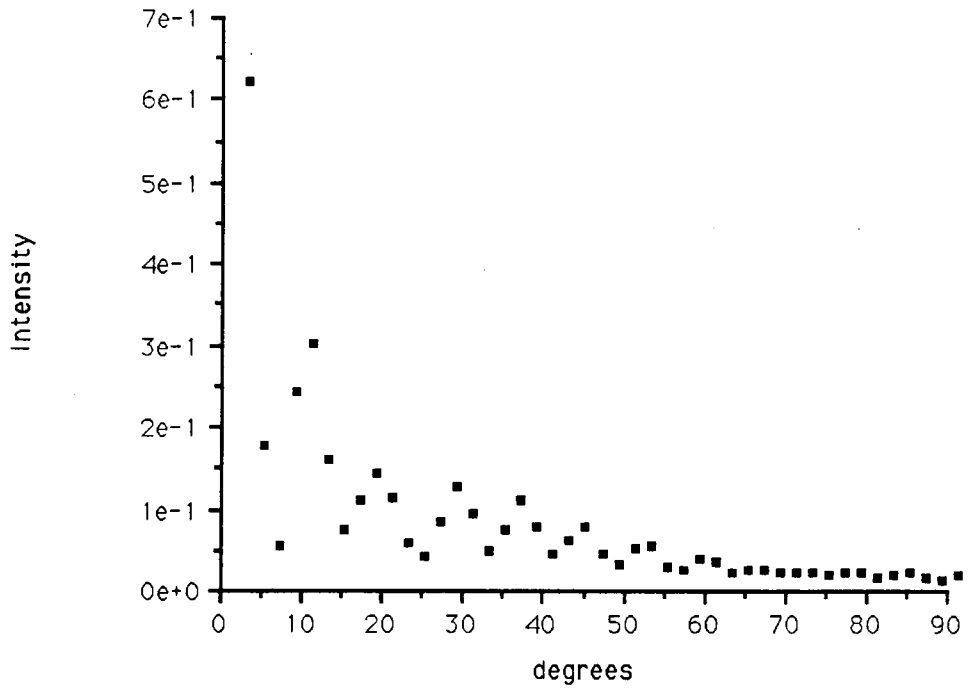


Figure 17. Theoretical Plot of Intensity Versus Angle for Glass Cylinders of 7 Micrometer Diameter

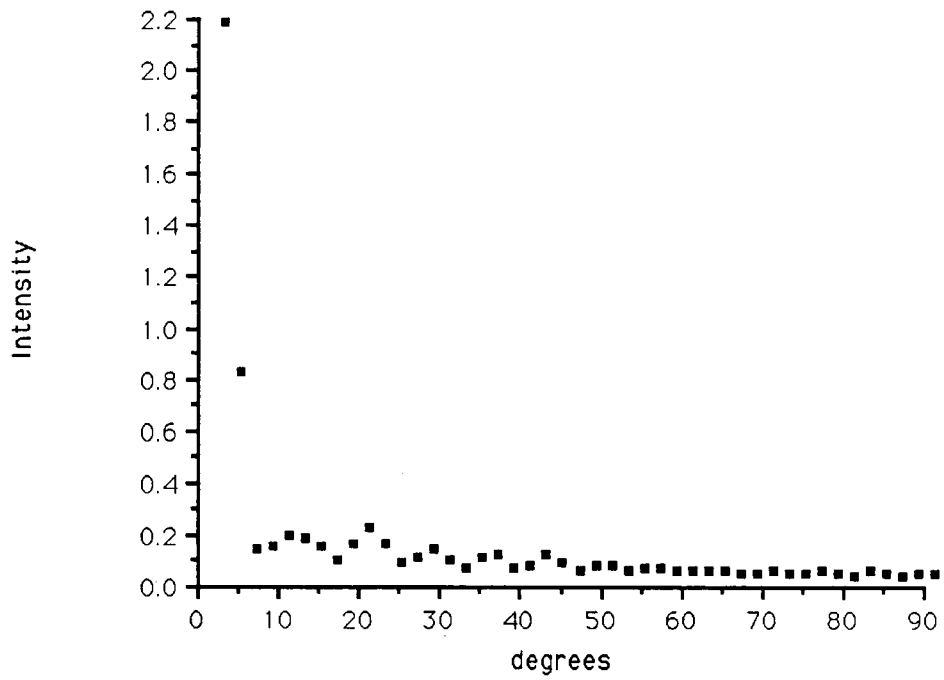


Figure 18. Theoretical Plot of Intensity Versus Angle for Glass Cylinders of 8 Micrometer Diameter

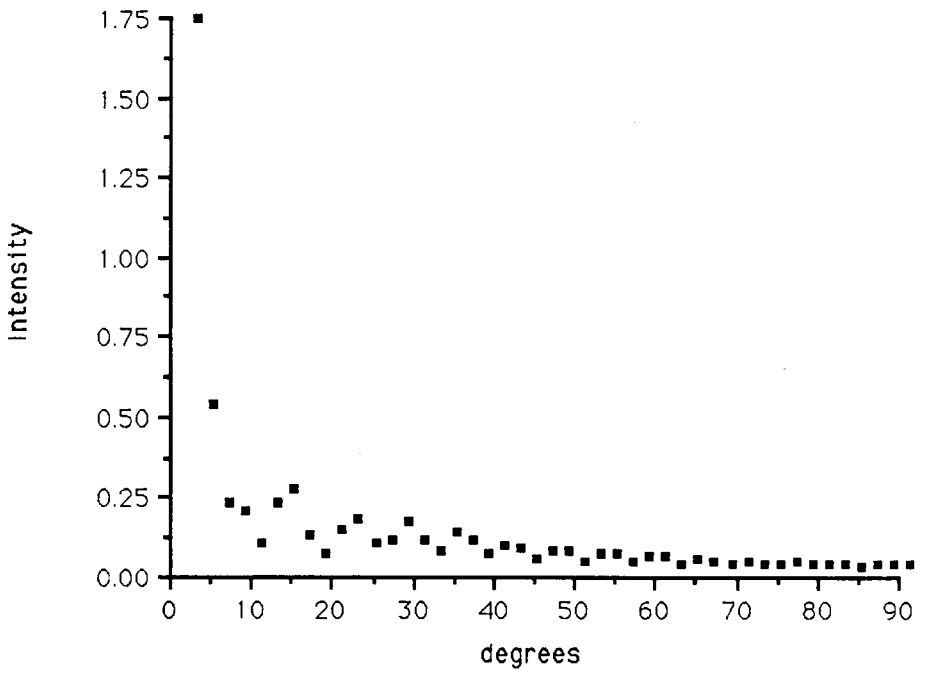


Figure 19. Theoretical Plot of Intensity Versus Angle for Glass Cylinders of 9 Micrometer Diameter

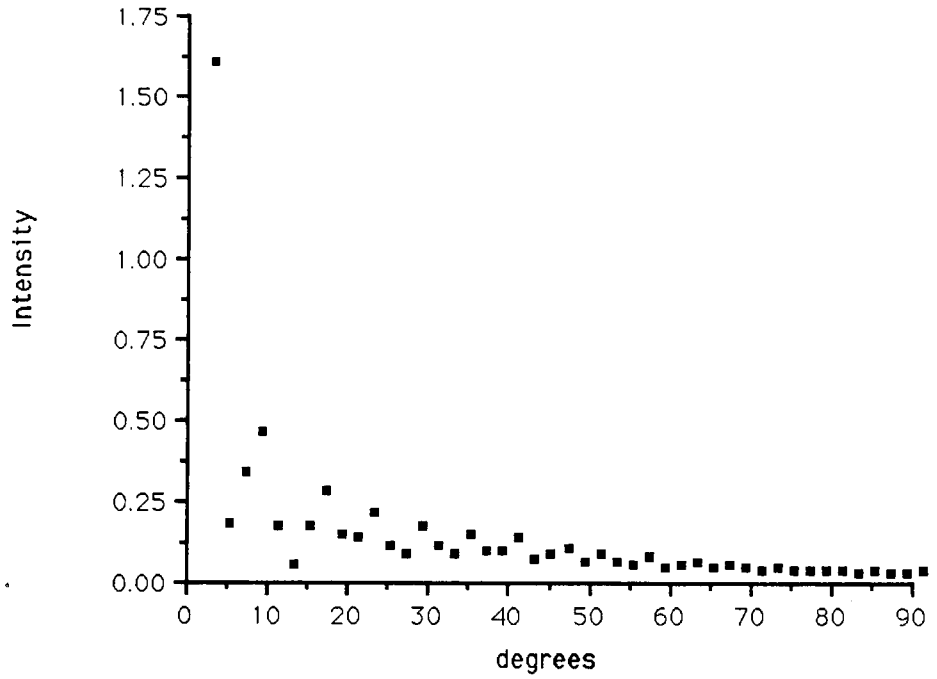


Figure 20. Theoretical Plot of Intensity Versus Angle for Glass Cylinders of 10 Micrometer Diameter

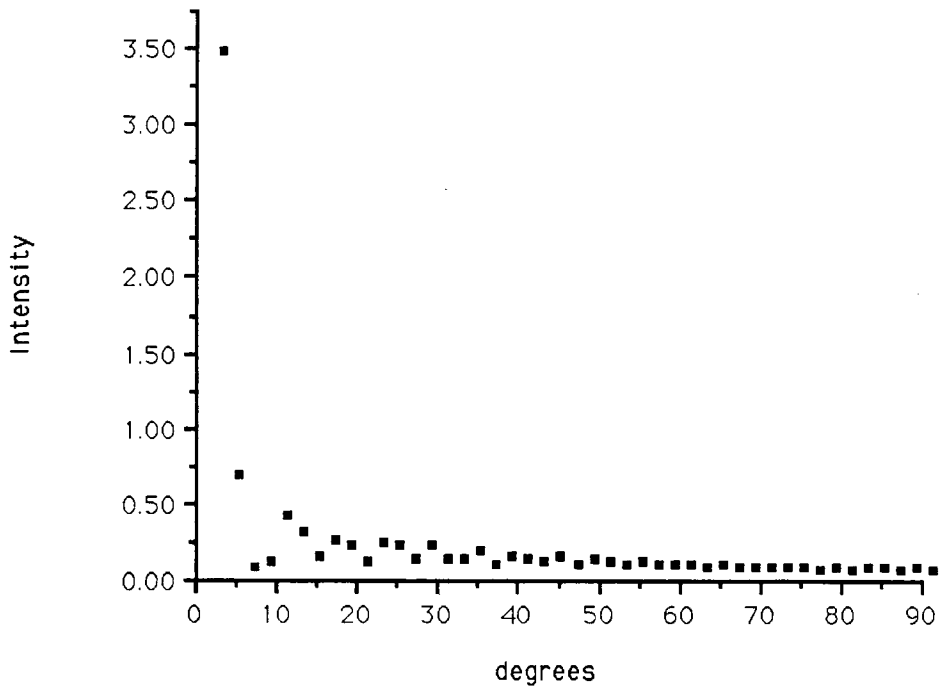


Figure 21. Theoretical Plot of Intensity Versus Angle for Glass Cylinders of 11 Micrometer Diameter

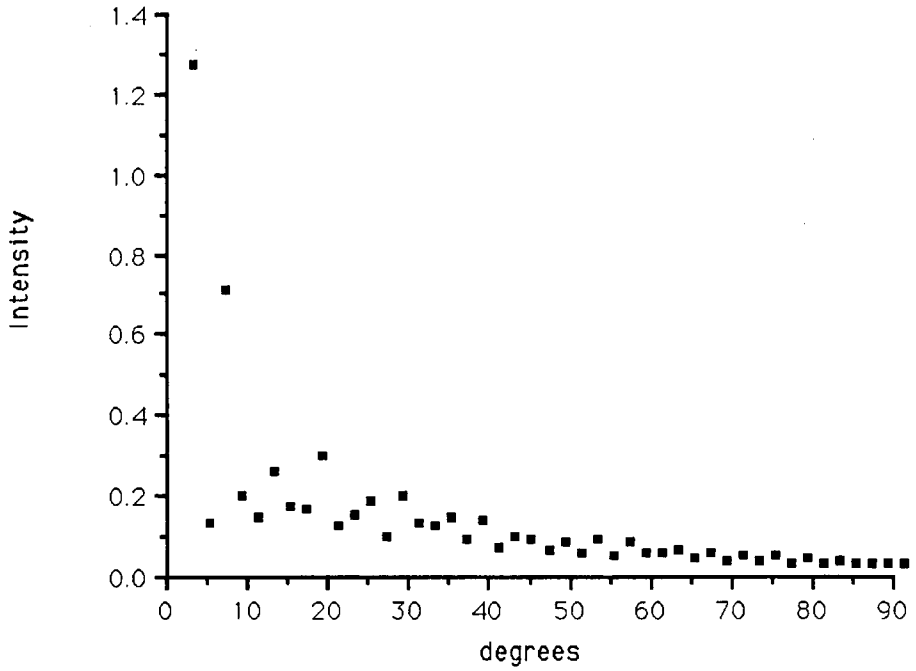


Figure 22. Theoretical Plot of Intensity Versus Angle for Glass Cylinders of 12 Micrometer Diameter

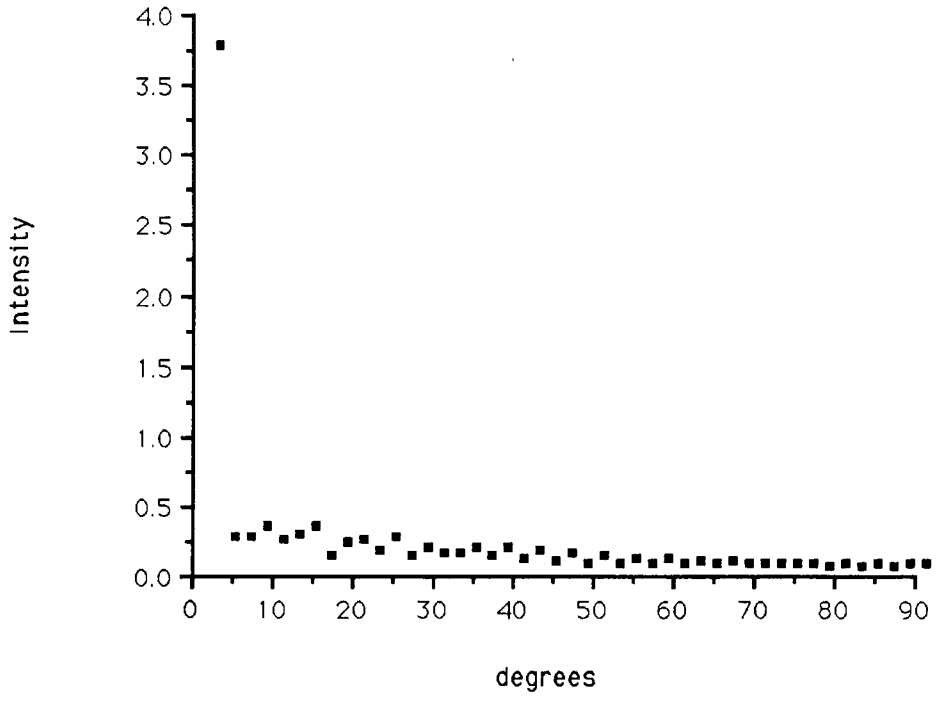


Figure 23. Theoretical Plot of Intensity Versus Angle for Glass Cylinders of 13 Micrometer Diameter

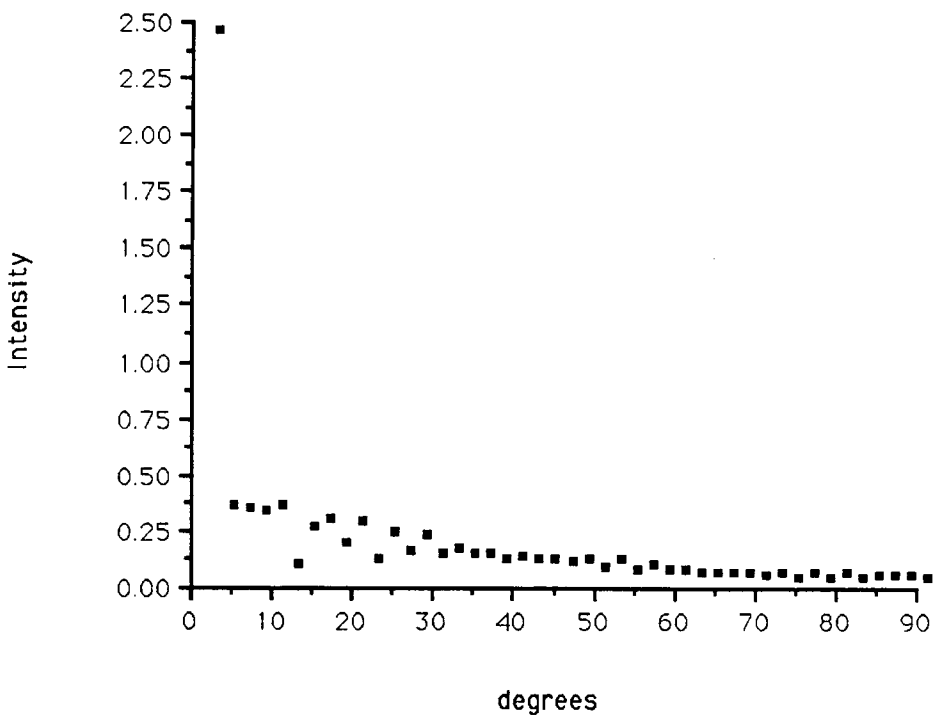


Figure 24. Theoretical Plot of Intensity Versus Angle for Glass Cylinders of 14 Micrometer Diameter

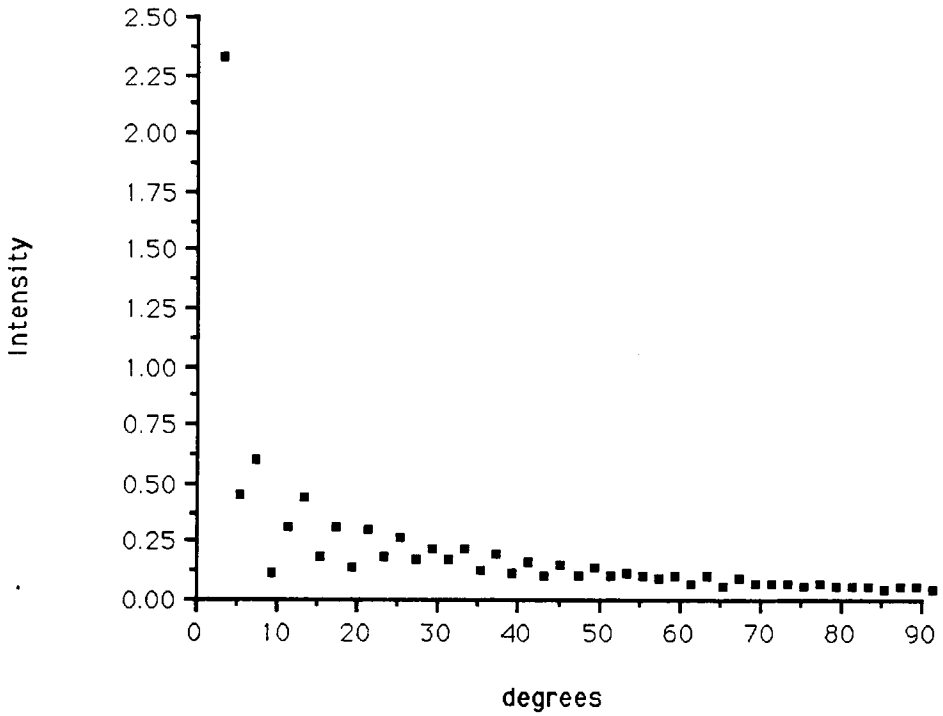


Figure 25. Theoretical Plot of Intensity Versus Angle for Glass Cylinders of 15 Micrometer Diameter

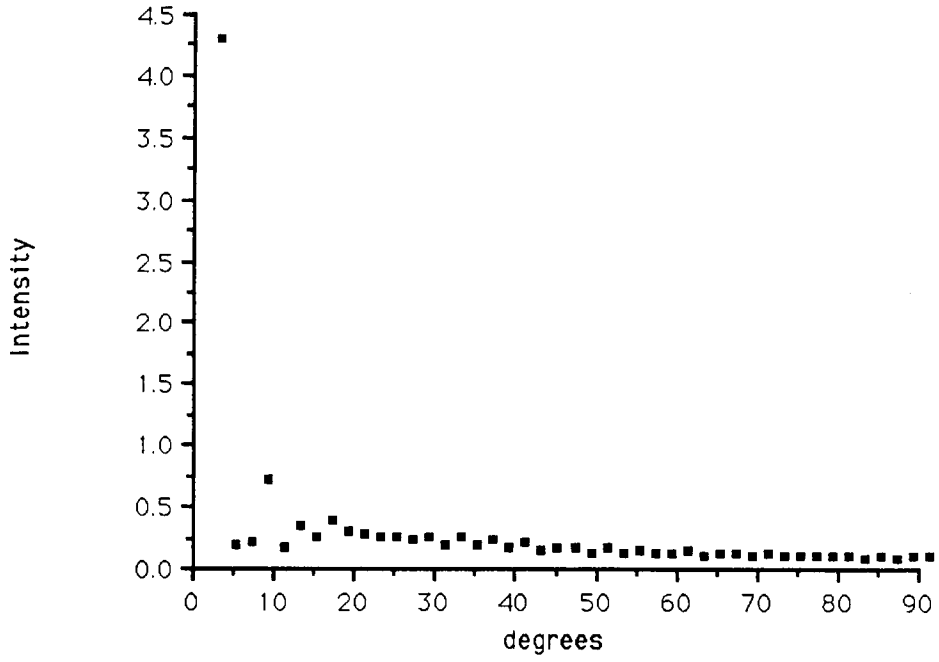


Figure 26. Theoretical Plot of Intensity Versus Angle for Glass Cylinders of 16 Micrometer Diameter

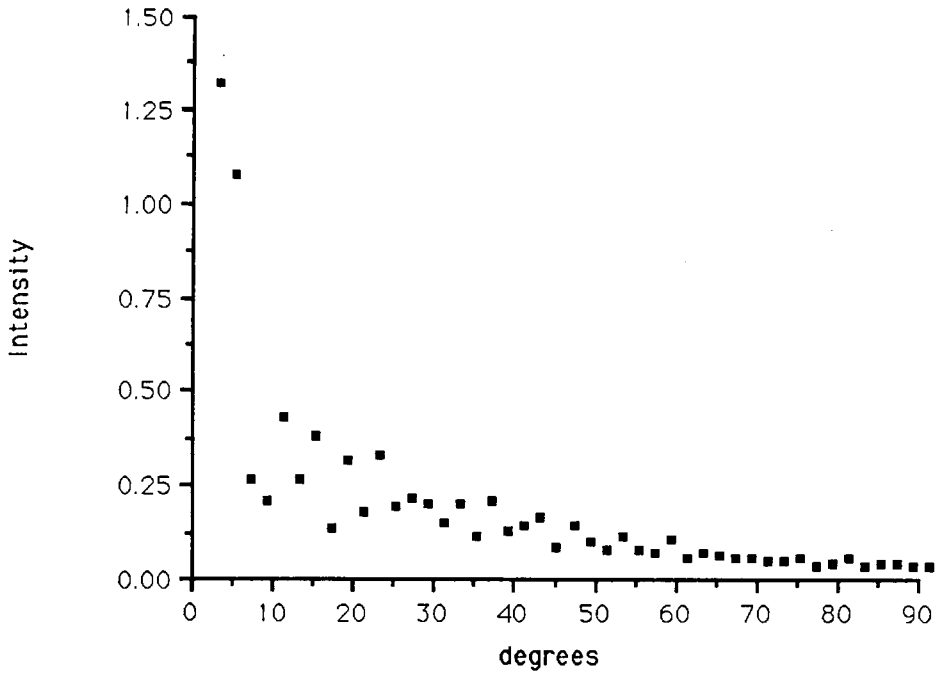


Figure 27. Theoretical Plot of Intensity Versus Angle for Glass Cylinders of 17 Micrometer Diameter

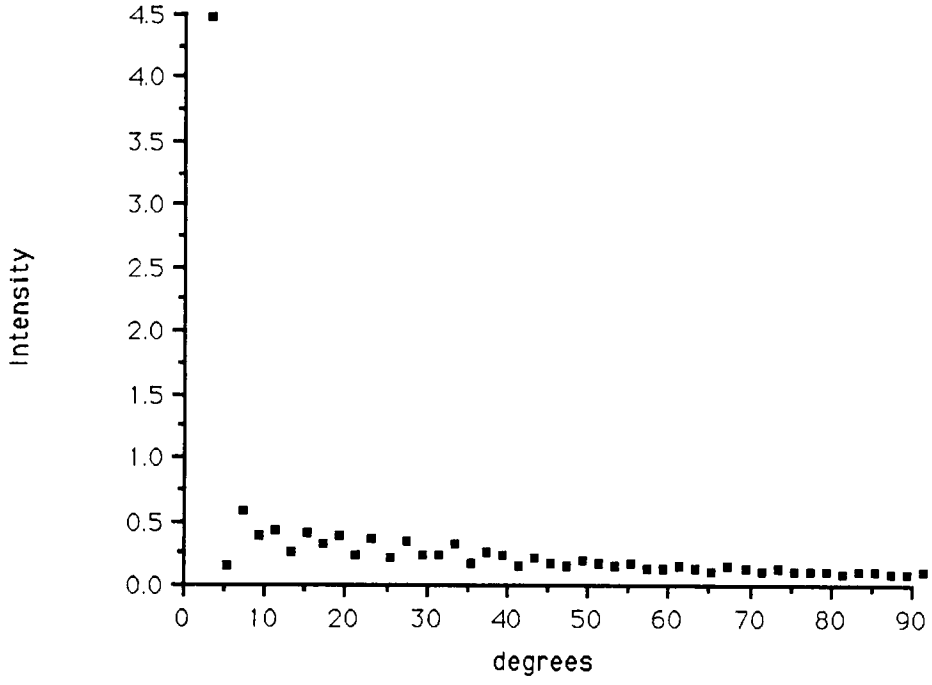


Figure 28. Theoretical Plot of Intensity Versus Angle for Glass Cylinders of 18 Micrometer Diameter

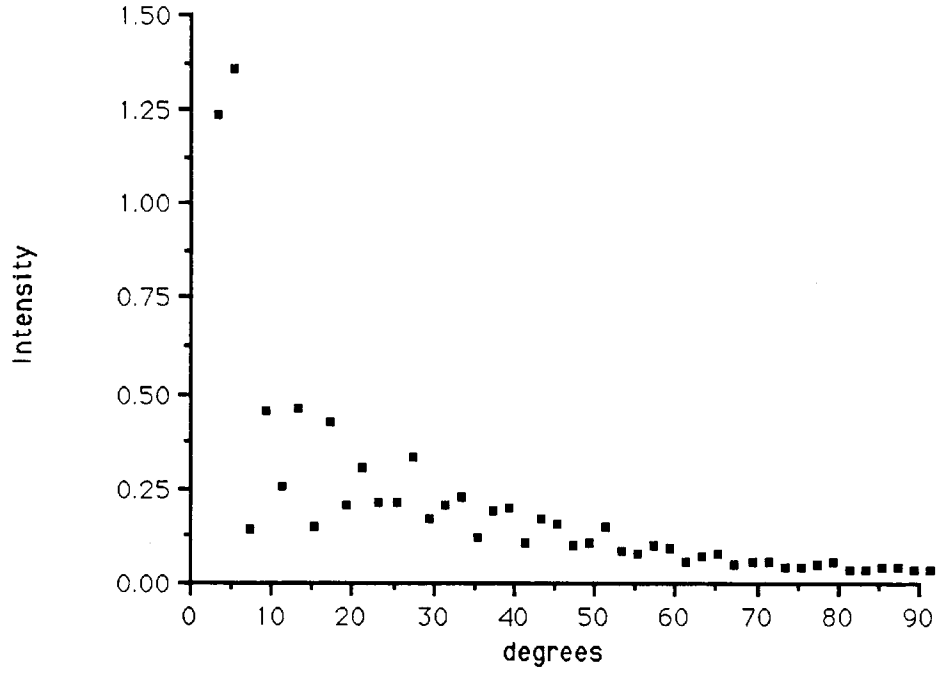


Figure 29. Theoretical Plot of Intensity Versus Angle for Glass Cylinders of 19 Micrometer Diameter

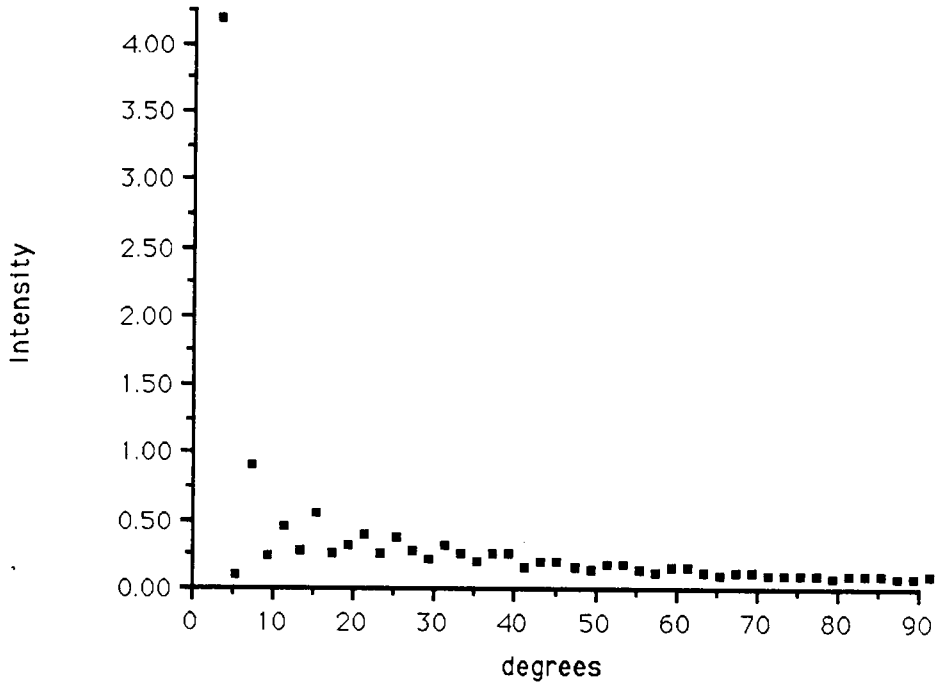


Figure 30. Theoretical Plot of Intensity Versus Angle for Glass Cylinders of 20 Micrometer Diameter

VITA

Harold H. Yount was born in Knoxville, Tennessee on February 25, 1965. He attended primary schools in both the Pittsburgh, Pennsylvania and Maryville, Tennessee school systems, and graduated from Maryville High School in 1983. He began his college career with a major in information and computer science at the Georgia Institute of Technology and participated in the cooperative engineering program. He did his field work at International Business Machines in Charlotte, North Carolina. In March of 1988, after having transferred to the University of Tennessee, he received the Bachelor of Science degree in electrical engineering. He was also a member of Eta Kappa Nu and a student member of the Institute of Electrical and Electronic Engineers.

Since December 1987, he has been employed by Schaffner Technologies Incorporated, Knoxville, Tennessee as a research and development engineer. During this time he has been working toward the Master of Science degree in electrical engineering at the University of Tennessee. In November 1988, he accepted a position as research engineer with Hewlett-Packard in Colorado Springs, Colorado.